Ore Geology Reviews 106 (2019) 97–112

Contents lists available at ScienceDirect

Ore Geology Reviews

journal homepage: www.elsevier.com/locate/oregeorev

Formation of chromitites and ferrogabbros in ultramafic and mafic members of the Variscan Ślęża ophiolite (SW Poland)

Piotr Marian Wojtulek[a,*], Bernhard Schulz[b], Katarzyna Delura[c], Michał Dajek[d]

[a] University of Wrocław, Institute of Geological Sciences, pl. Maksa Borna 9, 50-204 Wrocław, Poland
[b] TU Bergakademie Freiberg, Division of Economic Geology and Petrology, Institute of Mineralogy, Brennhausgasse 14, D-09596 Freiberg, Saxony, Germany
[c] University of Warsaw, Faculty of Geology, ul. Żwirki i Wigury 93, 02-089 Warszawa, Poland
[d] Ministry of Environment of the Republic of Poland, ul. Wawelska 52/54, 00-922 Warszawa, Poland

ARTICLE INFO

Keywords:
Ophiolite
Variscan
Ferrogabbro
Chromitite
Silicious inclusions
Spreading rate

ABSTRACT

Ultramafic and mafic rocks of the Variscan Ślęża ophiolite (Bohemian Massif, Sudetes, SW Poland) contain abundant Cr and Fe-Ti mineralizations. The occurrence of chromitites is related with serpentinites of refractory harzburgitic protoliths. Chromite I from chromitites has variable Cr and Mg numbers (Cr# = 0.41–0.58, Mg# = 0.62–0.83) and low TiO_2 contents (< 0.20 wt%). Chromite II surrounds chromite I or fills fissures in it and is enriched in Cr and depleted in Al relative to chromite I (Cr# = 0.54–0.68). Chromite I grains contain spherical grains of diopside, phlogopite, pargasite, pyrite and chalcopyrite, occurring as mono- or polyphase solid inclusions. Metagabbros with isotropic fabric contain locally up to 14.6 vol% of magnetite and ilmenite. Magnetite has variable TiO_2, Al_2O_3 and V_2O_3 contents (0.19–9.82 wt%, 0.13–1.67 wt% and 1.08–1.61 wt%, respectively). It forms xenomorphic grains with trellis or sandwich exsolutions of ilmenite, as well as aggregates with individual ilmenite grains.

The moderate Cr# of chromite I points to its origin from a MORB-type melt. The occurrence of hydrous inclusions and nodular textures indicates chromitite formation and alteration under low pressure conditions. Primary sulfide, phlogopite and pargasite inclusions suggest that the parental melt was moderately hydrous and sulphur-rich. Water in the magmatic system originated supposedly from interaction of primary MORB melt with hydrothermal fluids and a significant influence of fluids on chromite composition is expressed by its very low Ti content.

Metagabbros containing abundant Fe-Ti oxide mineralization may be classified as ferrogabbros. High V and Ti contents in magnetite indicate a magmatic origin. Its xenomorphic and intragrain mode of occurrence suggest crystallization between pre-existing gabbroic minerals like pyroxene and plagioclase. Ilmenite exsolutions indicate its growth at the expense of magnetite under oxidizing conditions. Occurrence of chromitites in harzburgites and ferrogabbros related to isotropic gabbros may suggest various spreading conditions during formation of the mafic and ultramafic members of the Ślęża ophiolite.

1. Introduction

Ophiolites are mafic-ultramafic massifs representing fragments of an ancient upper mantle and oceanic crust (Coleman, 1977). Their incorporation into orogens takes place due to continent-continent and arc-continent collisions, ridge-trench interactions or subduction-accretion events (Dilek and Furnes, 2011 and references therein). Ophiolitic massifs host various types of ore deposits. Primary deposits are related to magmatic and hydrothermal processes operating during the formation and emplacement of ophiolitic rocks (Coleman, 1977). They involve chromitites associated with ultramafics (e.g. González-Jiménez et al., 2014), Ti-Fe ore mineralizations related to gabbros (Natland et al., 1991) and massive sulfides restricted to extrusive volcanics (Coleman, 1977). Ophiolitic ore minerals (Cr-spinel, Fe-Ti oxides) are useful petrogenetic indicators, which provide information on parental magma chemistry, oxidation state and other crystallization conditions (Dick and Bullen, 1984; Ballhaus et al., 1990). Their occurrence and features depend on their position in the ophiolitic sequence and the structure of ophiolites, which is related to specific spreading rate conditions (Leblanc and Nicolas, 1992; Dick et al., 2000; Ahmed and Arai, 2002; Nicolas and Boudier, 2003). Presence of hydrous inclusions within chromite grains indicates also a significant influence of fluids on

* Corresponding author.
E-mail address: piotr.wojtulek@interia.pl (P.M. Wojtulek).

https://doi.org/10.1016/j.oregeorev.2019.01.021
Received 5 September 2018; Received in revised form 8 December 2018; Accepted 22 January 2019
Available online 24 January 2019
0169-1368/

formation of chromitite bodies (Lorand and Ceuleneer, 1989), as well as on formation of transitional harzburgite-dunite zone in the ophiolitic sequence (Rospabé et al., 2017).

This paper presents petrological and geochemical studies of Cr and Fe-Ti ore mineralizations from the Variscan Ślęża ophiolite (SW Poland). It is an unique ophiolitic sequence comprising a highly refractory harzburgitic mantle section with chromitites and a gabbroic section consisting mostly of isotropic rocks with ferrogabbroic intercalations. Occurrence of such mineralizations in the Ślęża ophiolite is puzzling because chromitites and ferrogabbros could be interpreted to have formed in various ophiolite types and spreading rates (Nicolas and Boudier, 2003; Leblanc and Nicolas, 1992; Dick et al., 2000). The aims of this article are (1) to interpret the origin of chromitites and their silicate solid inclusions, as well as Fe-Ti oxide accumulations related to metagabbros and (2) to show some contrasting features of the mafic and ultramafic members of the ophiolite.

2. Geology

The Ślęża massif is one of the mafic-ultramafic massifs interpreted to be the Central-Sudetic ophiolites (Narębski et al., 1982). They occur in the Central Sudetes, NE part of the Bohemian Massif, in a collage of crustal blocks or exotic terranes with contrasting geological evolution (Figs. 1a and b). These units were squeezed between the Saxo-Thuringia and Brunia microplates and supposedly represent the fragmented accretionary wedge (Mazur et al., 2015). The Central-Sudetic ophiolites are localized around the Sowie Góry Block, which consists of gneisses containing granulites and garnet peridotites metamorphosed under high temperature and ultra-high pressure (HT-UHP) conditions (Kryza and Pin, 2002). According to geophysical and tectonical studies, ophiolitic rocks dip beneath and underlie the Sowie Góry Block (Znosko, 1981).

The Ślęża ophiolite represents one of the best preserved and most complete fragments of Palaeozoic oceanic crust within the Variscan belt (Pin et al., 1988). Its pseudostratigraphic sequence (from S to N) consists of serpentinites, serpentinized rocks rich in pyroxene and amphibole, metagabbros, amphibolites and metamorphosed radiolarian cherts (Figs. 2 and 3, Majerowicz, 1979). These rocks are interpreted respectively as mantle peridotites, ultramafic cumulates, gabbros, a volcanic member (involving sheeted dyke complex and pillow lavas) and oceanic sediments (Majerowicz, 1979; Floyd et al., 2002). Previous works by Pin et al. (1988) demonstrated the N-MORB-type geochemical and Nd-Sr isotopic affinities of the gabbroic and volcanic rocks of the Ślęża and Nowa Ruda massifs, although these authors did not preclude a subduction-related setting. However, studies of melt percolation phases in serpentinized peridotites of the Ślęża and Braszowice-Brzeźnica massifs point to a transitional affinity between MORB and back-arc basin basalts (Wojtulek et al., 2016a, 2017).

The age of the ophiolitic rocks was estimated by various authors. Zircon dating of plagiogranites within the Ślęża gabbroic member by the conventional U-Pb method yielded a protolith age of 423 ± 20 Ma (Oliver et al., 1993). Abraded single zircon grains from the contact zone between rodingite dyke and serpentinite were analyzed by Dubińska et al. (2004). That U–Pb age of 400 +4/−3 Ma was interpreted as dating crystallization of zircon during metasomatic processes associated with serpentinization of peridotites of the Ślęża (Dubińska et al., 2004). More recently, U-Pb SHRIMP dating of zircons from metagabbroic and metavolcanic rocks yielded the ages of 400 ± 10 Ma and 403 ± 6 Ma, related to magmatic crystallization of rocks forming plutonic and volcanic members of the Ślęża ophiolite (Kryza and Pin, 2010).

2.1. Ultramafic rocks

The ultramafic member of the Ślęża ophiolite comprises heavily

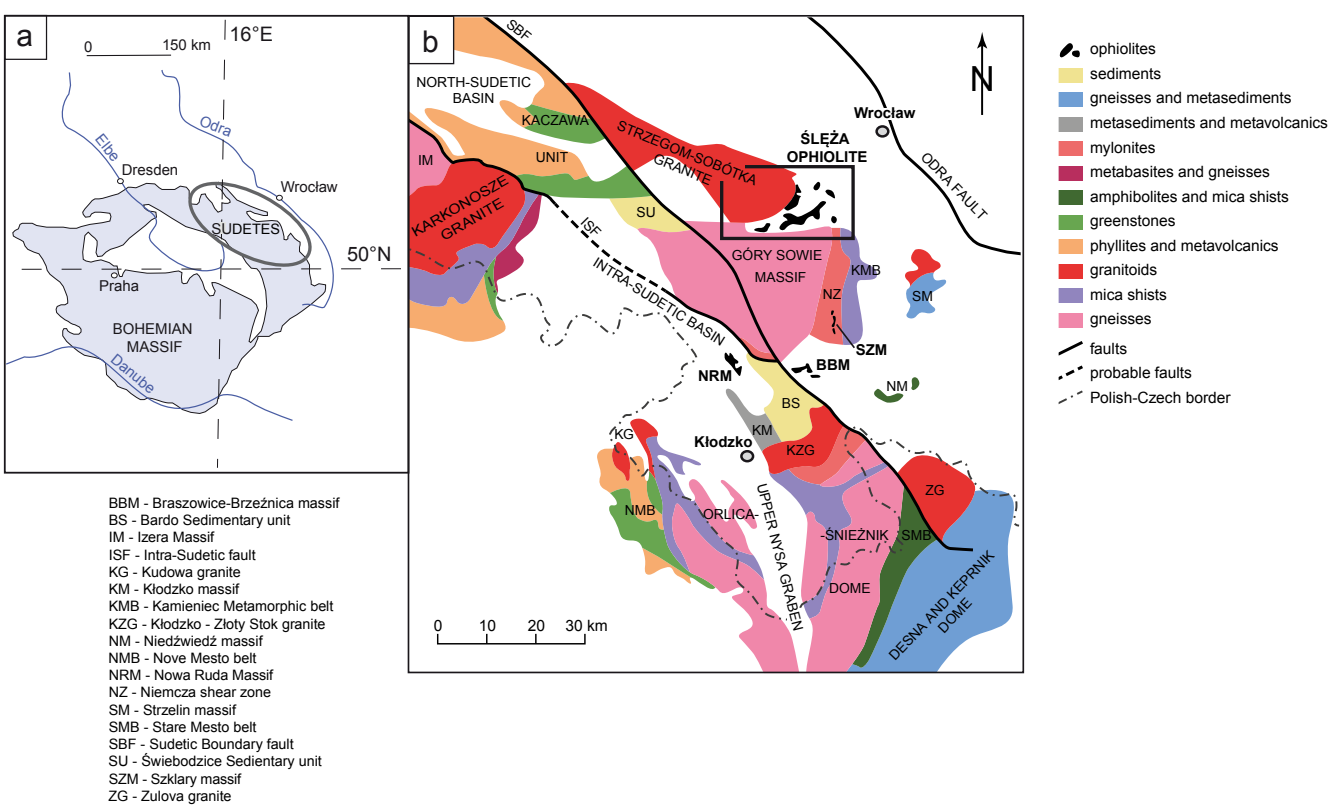

Fig. 1. a – Location of Sudetes within the Bohemian Massif in Central Europe. b – Position of the Ślęża Ophiolite relative to major geological units of Sudetes, modified from Mazur et al. (2015).

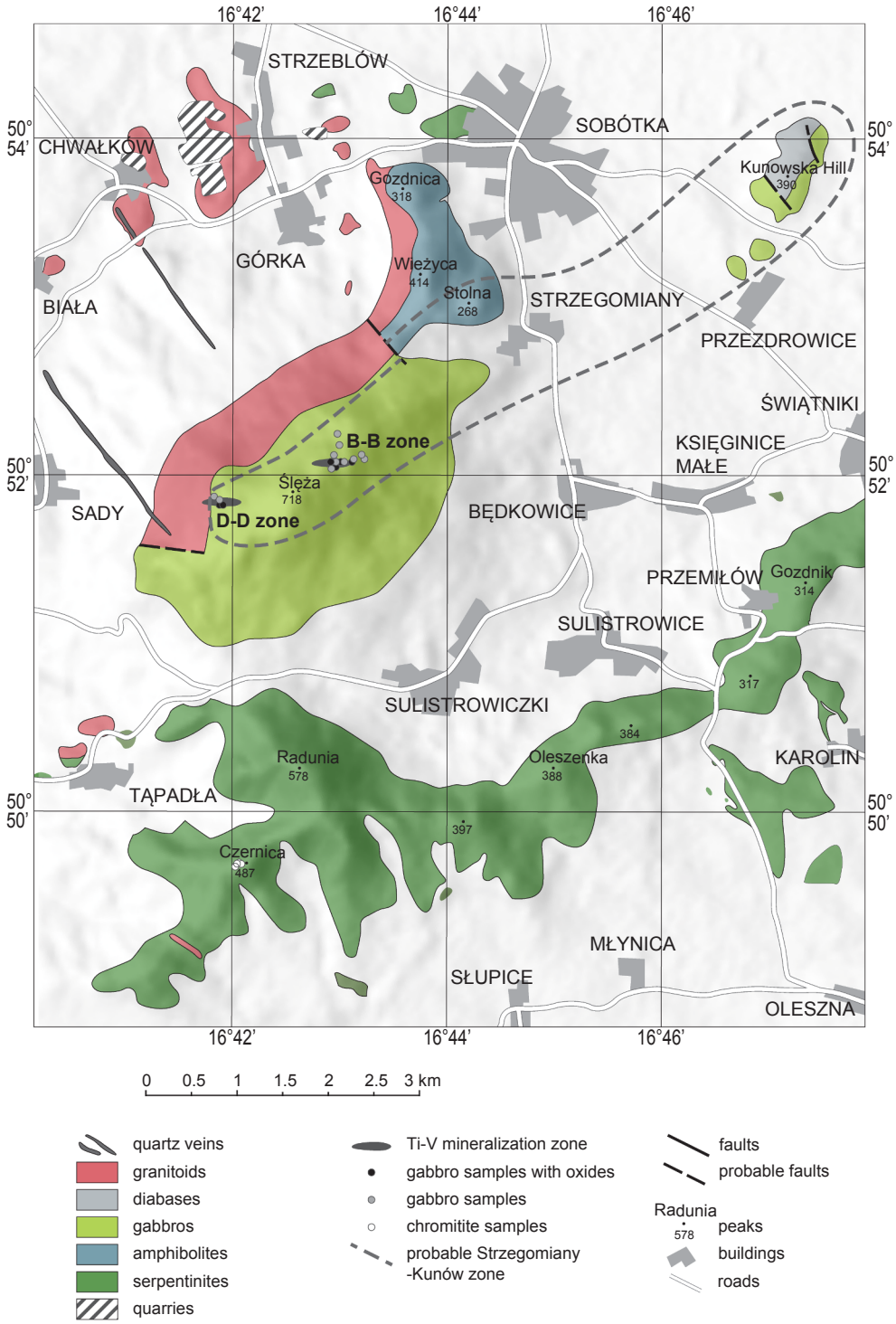

Fig. 2. Geological sketch map of the Ślęża Ophiolite (based on the map of Majerowicz, 2006).

serpentinized rocks (Figs. 2 and 3). Serpentinites occur as pseudomorphic or non-pseudomorphic varieties with various amounts of the non-serpentine minerals. Ultramafic rocks neighboring the gabbroic outcrops (the Radunia and Czernica Hills – Fig. 2) are rich in olivine–clinopyroxene–chromite aggregates, whereas other rocks (in the Oleszenka and Gozdnik Hills) are completely serpentinized. Although the whole rock normative compositions of the serpentinites indicate harzburgite and subordinate dunite protoliths, they contain neither orthopyroxene nor residual clinopyroxene. Interstitial clinopyroxene from olivine-clinopyroxene-chromite aggregates has distinctly lower Al_2O_3 and Cr_2O_3 contents (2.20–4.00 wt% and 0.80–1.40 wt%, respectively) than residual clinopyroxene typical for abyssal peridotites. Its interstitial mode of occurrence and composition is similar to melt impregnation phases originating from the basaltic melt percolation through peridotite (Wojtulek et al., 2016a).

A metamorphic evolution of the serpentinites involved the following stages: (1) alteration of peridotite due to ocean floor metamorphism and formation of pseudomorphic texture of serpentinites, indicative of low-T conditions (bastite and mesh textures after pyroxenes and olivine with abundant magnetite), (2) high-T recrystallization of

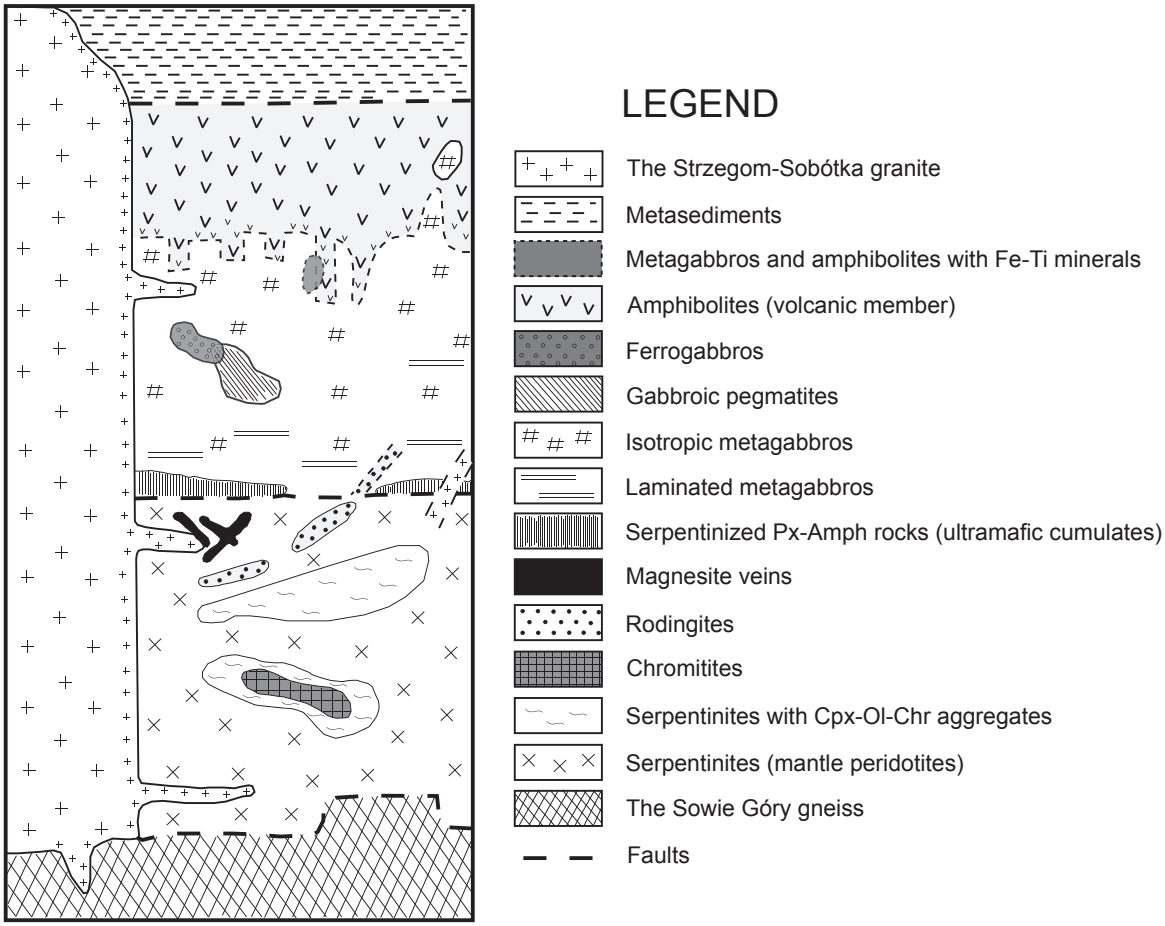

Fig. 3. Ideal stratigraphic outline of the Ślęza ophiolite sequence (modified from Majerowicz, 2006).

pseudomorphic serpentines, which were replaced by high-T, non-pseudomorphic antigorite rosette crystals (Dubińska and Gunia, 1997) and (3) dehydration of serpentine phases and formation of magnetite-bearing olivine and clinopyroxene, which mark an increasing degree of alteration (Wojtulek et al., 2016a).

2.2. Chromitites

Podiform type chromitites occur within serpentinites containing melt impregnation olivine-clinopyroxene-chromite aggregates on the Czernica Hill, ~1500 m below the paleo-Moho of the Ślęża ophiolite (Fig. 2). They form veins and pockets with stock-type morphology and irregular boundaries. The ore bodies are elongated in a NE-SW direction and the fabric of the ores mimics this elongation trend (Spangenberg, 1944). The mined pockets were 8–12 × 4–3 × 2–4 m in size, whereas the veins were up to 22 m long and up to 2 m wide (Birecki, 1962). Ore bodies are typically surrounded by alteration zones (salbands) containing less chromian spinel (Spangenberg, 1943). Chromian ore occurs as the following varieties: (1) massive ore, (2) laminated ore, (3) nodular ore, (4) disseminated ore, (5) brecciated ore and (6) chromitite veinlets within serpentinite (Delura, 2012). Particular types of chromitite ore contain between 30 and 90 vol% of chromite. Chromitites are very poor in platinum-group elements, they contain 42–79 ppb of total PGEs (Wojtulek et al., 2016b).

Chromitites from the Ślęża consist of high-Al chromite I (Cr# = 0.50–0.52, Mg# = 0.60–0.70), high-Cr chromite II (Cr# = 0.57–0.69, Mg# = 0.39–0.63), ferritchromite and chlorite. Chromite I represents supposedly a primary phase of chromitites, whereas occurrence of chromite II, ferritchromite and chlorite is a result of the greenschist-facies metamorphic overprint (Delura, 2012). A secondary genesis is also suggested for sulfides (millerite, godlevskite and polydymite) occurring within chlorite (Wojtulek et al., 2016a). However, previous publications concerning the Ślęża chromitites did not describe silicate solid inclusions within chromite (except for rare clinopyroxene and olivine inclusions), thus interpretation of their origin could not be complete.

2.3. Gabbroic rocks

The Ślęża gabbroic body is ~12 km long and ~6 km wide. Contacts between metagabbros and serpentinites (to the south) and between metagabbros and metabasalts (to the north) are intrusive and locally tectonic (Majerowicz, 2006). To the west, metagabbros are in intrusive contact with younger biotite granodiorite of the Strzegom-Sobótka massif, dated at 299.3 ± 2.4 Ma (Turniak et al., 2014). The plutonic member of the Ślęża ophiolite comprises medium- to coarse-grained, mostly isotropic rocks. Locally, metagabbros display an igneous, ophitic or subophitic texture. The occurrence of leuco- and melanocratic kinds of metagabbros as well as gabbroic pegmatoids is random. Rocks displaying macrorhytmic magmatic layering defined by an alternation of light (plagioclase-rich) and dark (clinopyroxene-rich) cm-scale bands occur mostly in the vicinity of the paleo-Moho (Abdel Wahed, 1999).

Rocks belonging to the gabbroic member of the Ślęża ophiolite are only selectively and not penetratively deformed (Majerowicz, 2000). The gabbros were altered under the greenschists and lower amphibolite facies metamorphism, which caused advanced saussuritization of plagioclase and replacement of pyroxene by secondary Mg-hornblende and actinolite (Kryza and Pin, 2010). The same conditions apply to the alteration of metabasalts of the Ślęża ophiolite (Kryza and Pin, 2010).

Table 1
Whole-rock major (wt%) and trace (ppm) element analyses of metagabbros from the Ślęża ophiolite.

Sample Rock type	Detection limit	Złomiska TV07 Metagabbro with ore mineralization	Złomiska TV08a Metagabbro with ore mineralization	Olbrzymki OL3 Gabbroic pegmatite with ore mineralization	Złomiska TV09 Isotropic metagabbro	Złomiska TV20 Isotropic metagabbro	Olbrzymki OL4 Isotropic metagabbro	Tąpadła valley G20 Laminated metagabbro	Tąpadła valley PW15 Laminated metagabbro
SiO_2	0.01	43.59	43.76	46.88	49.79	48.36	49.94	48.83	49.09
TiO_2	0.01	4.01	4.28	2.10	0.61	0.43	0.39	0.45	0.25
Al_2O_3	0.01	12.82	12.35	16.57	17.46	17.60	18.55	14.72	15.78
Cr_2O_3	0.01	< 0.002	< 0.002	0.02	0.04	0.08	0.06	0.05	0.06
Fe_2O_3*	0.01	20.29	20.12	12.17	6.31	6.61	7.88	8.08	5.82
MnO	0.01	0.25	0.28	0.17	0.13	0.12	0.12	0.14	0.10
MgO	0.01	6.20	6.37	7.27	6.54	9.60	7.30	10.79	10.03
CaO	0.01	8.97	9.18	10.27	14.24	12.90	10.94	12.83	11.97
Na_2O	0.01	2.51	2.37	3.18	2.69	2.26	3.43	1.94	2.90
K_2O	0.01	0.10	0.10	0.10	0.17	0.12	0.10	0.12	0.06
P_2O_5	0.01	0.02	0.04	< 0.01	0.07	0.01	0.02	< 0.01	< 0.01
LOI	–	0.90	0.80	1.00	1.80	1.70	1.10	1.80	3.70
Sum	–	99.64	99.66	99.76	99.81	99.78	99.83	99.75	99.76
Be	1.0	< 1	< 1	< 1	< 1	1	< 1	< 1	< 1
Sc	1.0	43	49	42	39	42	31	50	50
V	8.0	1116	1011	222	161	458	141	220	187
Co	0.2	64	63	28	39	45	39	48	37
Ni	0.1	36	26	59	133	44	90	117	97
Ga	0.5	20.80	19.90	16.10	12.90	16.50	16.00	12.60	11.60
Rb	0.1	1.20	2.40	9.20	3.60	2.10	2.10	2.90	1.20
Sr	0.5	129	120	282	186	160	174	110	169
Y	0.1	20.40	23.80	18.60	10.20	22.20	8.70	10.80	5.00
Zr	0.1	42.40	54.10	31.60	12.60	39.40	10.10	10.50	1.60
Nb	0.1	0.50	1.00	0.10	< 0.10	0.20	< 0.10	0.20	< 0.10
Cs	0.1	< 0.10	< 0.10	0.10	< 0.10	< 0.10	< 0.10	< 0.10	0.10
Ba	1.0	7	8	41	19	9	13	8	8
La	0.1	1.90	1.50	3.30	1.00	1.20	1.00	0.50	0.20
Ce	0.1	4.50	4.80	4.40	2.00	4.30	1.40	1.50	0.30
Pr	0.02	0.79	0.96	1.15	0.36	0.75	0.32	0.30	0.04
Nd	0.03	4.40	5.70	5.50	2.00	5.10	2.00	1.90	0.40
Sm	0.05	1.73	2.24	1.78	0.79	1.80	0.63	0.95	0.35
Eu	0.02	1.00	1.21	0.98	0.51	1.19	0.73	0.61	0.26
Gd	0.05	2.82	3.64	2.75	1.44	3.08	1.28	1.57	0.66
Tb	0.01	0.51	0.66	0.50	0.27	0.56	0.23	0.29	0.15
Dy	0.05	3.54	4.49	3.30	1.81	3.91	1.70	1.96	0.87
Ho	0.02	0.74	0.96	0.70	0.36	0.82	0.36	0.43	0.19
Er	0.1	2.30	2.82	2.08	1.10	2.38	1.17	1.27	0.53
Tm	0.01	0.31	0.37	0.27	0.14	0.30	0.14	0.18	0.07
Yb	0.05	1.95	2.54	1.80	0.93	2.15	0.91	1.13	0.47
Lu	0.01	0.32	0.37	0.27	0.15	0.33	0.13	0.17	0.07
Hf	0.1	1.30	1.60	1.00	0.40	1.20	0.40	0.40	0.20
Ta	0.1	< 0.10	0.10	< 0.10	< 0.10	< 0.10	< 0.10	< 0.10	< 0.10
W	0.5	< 0.50	< 0.50	< 0.50	< 0.50	< 0.50	< 0.50	0.50	< 0.50

* Total Fe as Fe_2O_3.

2.4. Fe-Ti Mineralization

First pointed out on a map by Finckh (1928), abundant Ti-Fe ore mineralization occurs in metagabbros, metadiabases and metabasalts in an elongated area between the peak of the Ślęża mountain and the village of Kunów (Fig. 2, Jamrozik et al., 1988; Niśkiewicz and Siemiątkowski, 1993, Abdel Wahed and Mierzejewski, 2000). These rocks occur in an area ~7 km long and ~2 km wide (the Strzegomiany – Kunów zone) and their occurrence is related to a magnetic anomaly of amplitudes ranging from 1000 to 2000 nT (Cholewicka – Meysner et al., 1989). Ti-ore mineral contents in the mafic rocks is variable: metagabbros from Strzegomiany contain 4.4–12.2% vol. (Niśkiewicz and Siemiątkowski, 1993), whereas metabasalts from Kunów have up to 12.1% vol. of magnetite and ilmenite (Majerowicz, 2000). Despite the overall poor exposure of rocks in the Ślęża, metagabbros abundant in Fe-Ti oxides are exposed in situ in the B-B and D-D mineralization zones (Abdel Wahed and Mierzejewski, 1998). The former is ~25 m long and ~15 m wide, whereas the latter is ~8 m long and up to 2 m wide. The contact between rocks containing Ti-Fe ore minerals and those without ore mineralization is sharp and dips towards the SSE (Abdel Wahed and Mierzejewski, 1998). The B-B and D-D zones are elongated in a SW-NE direction, similar to the elongation of the whole Strzegomiany-Kunów zone.

3. Analytical data

This study is based on 10 samples of chromitites and 34 samples of metagabbros. Chromitite samples were collected from two dumps located in the vicinity of abandoned shafts on the Czernica Hill. In situ sampling and direct observations of chromitites were not possible due to the destruction of mines and the lack of chromitite outcrops. We have selected only 10 nodular, inclusion-bearing chromitites from 110 samples collected in years 2002–2016, because silicate inclusions in chromitites are very scarce. Metagabbro samples were collected from outcrops located in the B-B and D-D mineralization zones in the vicinity of the Ślęża mountain peak and in the Tąpadła valley.

3.1. Whole rock characterization

We determined whole rock compositions of nodular chromitites,

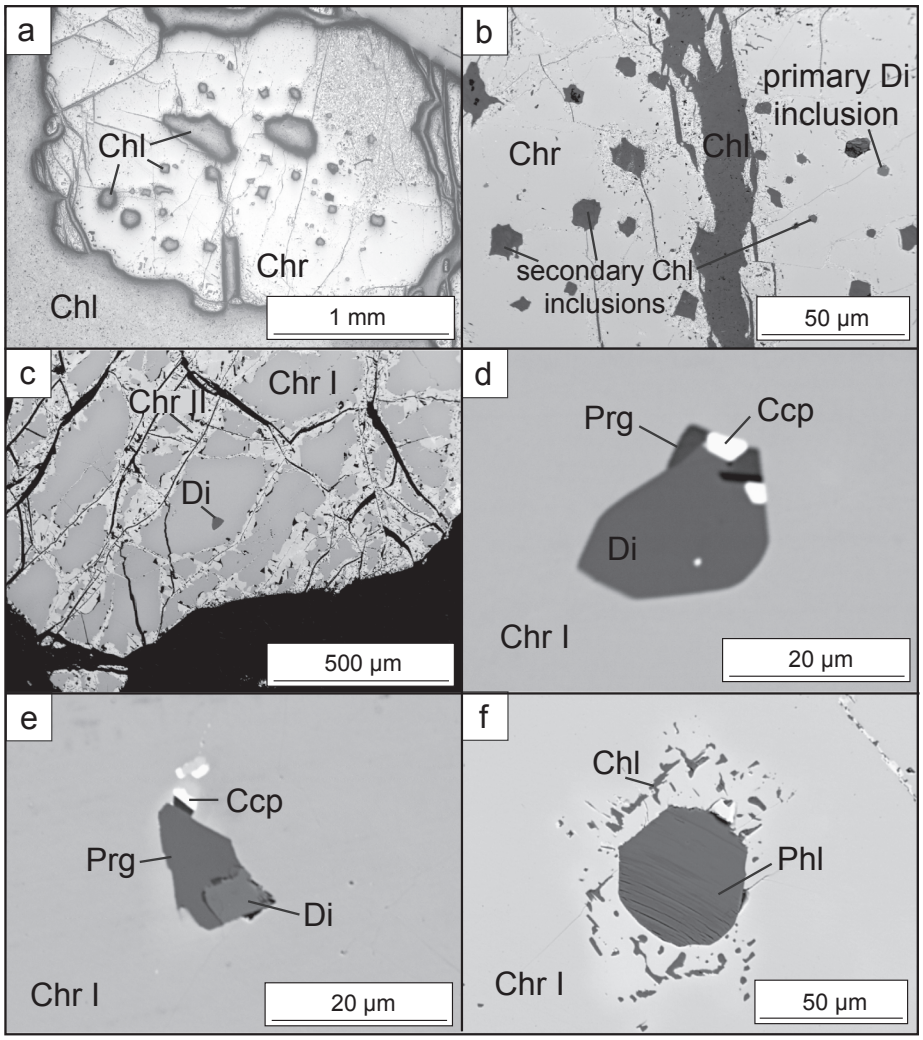

Fig. 4. Photomicrographs of solid inclusions within chromitites occurring in the Czernica Hill area. a – Chromite grain containing numerous chlorite inclusions, reflected light image (TAAII). b – Chromite grain cut by chlorite. Solid inclusions within chromite comprise chlorite and diopside, BSE image (TAP). c – Chromite grain consisting of chromite I (high-Al) and chromite II (high-Cr) with diopside inclusion, BSE image (TAA). d – Polyphase inclusion consisting of diopside, pargasite and chalcopyrite, BSE image (TAP). e – Polyphase inclusion consisting of pargasite and diopside, BSE image (TAP). f – Spherical phlogopite inclusion within chromite I, BSE image (TAP).

metagabbros rich in Fe-Ti oxides, isotropic and laminated metagabbros. Fifteen samples were crushed and then pulverized in an agate mill at Bureau Veritas Analytical Laboratory in Vancouver, Canada. For the analytical procedures we used 200 mg samples. The whole rock characterization of samples was determined by inductively coupled plasma emission spectrometry (ICP-ES – for a major element composition) and inductively coupled plasma mass spectrometry (ICP-MS – for a minor and trace element compositions, minimum detection limits are given in Table 1). The whole rock composition of platinum group elements (PGEs) in ferrogabbros and chromitites (4 samples analysed) was determined at the Maxxam Analytics International Corporation in Mississaugua, Canada, by the neutron activation analysis. Minimum detection limits were: 1 ppb for Ir, 5 ppb for Rh, 10 ppb for Os, 20 ppb for Pd and Pt and 50 ppb for Ru.

3.2. EMP analysis

We used 150 µm thick sections for microscopic and chemical study. Polished thin sections of the samples were first studied by polarized optical microscope. Major- and minor-element compositions of minerals from 3 metagabbro samples have been analysed with a JEOL JXA 8900 electron microprobe at the TU Bergakademie Freiberg, Germany under standard conditions: acceleration voltage 15 kV, beam current of 20nA, and various counting times between 20 and 50 s on peak, dependent on the expected element concentrations. Natural silicates, synthetic oxides and metals were used as standards. The ZAF correction procedures supplied by JEOL were applied. Chromitite analyses (8 samples) were conducted using the Cameca SX-100 electron microprobe at Faculty of Geology, University of Warsaw, Poland. Standard conditions were applied (acceleration voltage 15 kV, sample current 15nA, counting times 10 or 20 s, natural silicates and synthetic oxides as standards) and the PAP correction procedure was used (Pouchou and Pichoir, 1984).

The structural formulae of minerals were recalculated on the basis of 4O for olivine, 23O for pargasite, 6O for clinopyroxene and 3 cations for spinel. Chromium number, Cr#, is defined as atomic 100 × Cr/(Cr + Al) and magnesium number, Mg#, as atomic 100 × Mg/(Mg + Fe^{2+}) in mineral formulae. Mineral abbreviations follow Siivola and Schmid (2007).

3.3. SEM-based automated mineralogy

Eight thin sections were analysed with a Mineral Liberation Analyzer (MLA), one of the methods of automated mineralogy (Fandrich et al., 2007). The MLA mapping of mineral grains was conducted using the FEI Quanta 650F field emission scanning electron microscope (FE-SEM) with two Bruker Quantax X-Flash 5030 energy-dispersive X-ray (EDX) detectors. The acceleration voltage of the electron beam was 25 kV and the beam spot was 10 nA. For data processing, the software version MLA Suite 3.1.686 was used. The grain-based X-ray mapping (GXMAP) method was applied to distinguish the particular minerals. The GXMAP routine produces a narrow grid of ~1600 EDX-ray spectra per mm^2 to cover the complete thin section. For the classification of minerals, a list of identified reference EDX-ray spectra was

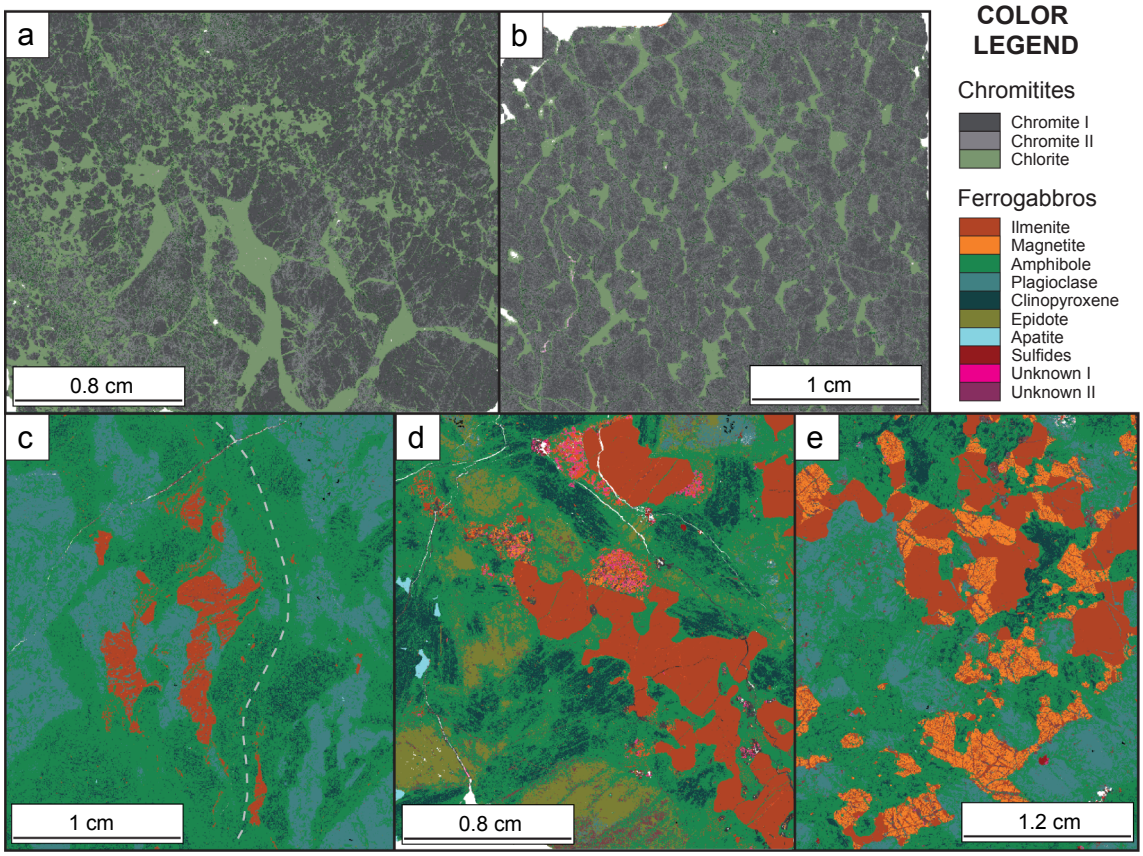

Fig. 5. Maps of energy dispersive X-ray (EDX) spectra. a – Brecciated chromitite containing primary solid inclusions (TAA). b – Brecciated chromitite containing primary solid inclusions, developed from nodular ore (T1). c – Deformed metagabbro containing ilmenite aggregate (OL3). d – Ferrogabbro containing coarse, xenomorphic ilmenite aggregates (TV17). e – Magnetite-ilmenite aggregates in ferrogabbro (TV07).

established by collecting the spectra of particular phases. The GXMAP measurements were classified against the reference EDX-ray spectra list with a high degree of probability of match and with an algorithm marking the non-matching spectra as an unknown. Therefore, the classified spectra represent semi-quantitative compositional data. In the last step, mineral phases were ordered by labelling with a color scale for visualization of their distribution in the thin section.

The second SPL (sparse phase liberation) routine was used for the detection of rare phases occurring as silicate, base metal and PGE inclusions in chromitites. This method combines a backscattered electron grey colour value trigger and single spot EDX-ray spectra analysis. It enables us to distinguish single grains of the searching phases searched for and then to analyse them by electron microprobe.

3.4. SEM-based element mapping

Quantitative element distribution maps of Cr-spinel grains were acquired in the Cryo-SEM/NanoFun laboratory, Faculty of Geology, University of Warsaw (Poland) using a Zeiss Auriga™ scanning electron microscope SEM-FE (field emission) equipped with two EDS detectors XFlash|30 produced by Bruker. An acceleration voltage of 15 kV and a 120 µm aperture were applied.

4. Petrography and chemical data

4.1. Petrography and chemistry of minerals

4.1.1. Chromitites and their solid inclusions

Chromitites from the Ślęża consist mostly of automorphic, coarse chromite grains up to 1.2 cm in diameter. These grains are irregularly fractured, locally their brecciation degree is very high (Figs. 4 and 5). They consist of highly aluminous chromite I of variable composition (Cr# = 0.41–0.58, Mg# = 0.62–0.83, Figs. 6 and 7, Table 2) and low TiO_2, V_2O_3, MnO and NiO contents (< 0.20, < 0.24, < 0.34 and < 0.25 wt%, respectively). Chromite I displays zonation, its cores are richer in Fe and poorer in Mg relative to the marginal parts of grains (Fig. 7). Other elements (Ti, Al and Cr) do not display zonation. Chromite I is surrounded or cut by high chromian chromite II (Cr# = 0.57–0.70, Mg# = 0.55–0.68) and ferritchromite.

Numerous solid inclusions of various sizes (10–200 µm) occur in the nodular or brecciated chromitites. Chromite grains contain either single or numerous, randomly distributed inclusions (Fig. 4). They are filled mostly by secondary chlorite forming coarse, up to 0.5 mm inclusions (Fig. 4a and b), which is poorer in Al relative to chlorite filling interstices between chromite grains (averaged 22.07 wt% and 18.35 wt% Al_2O_3, respectively). Part of chlorite grains form also minute inclusions surrounding phlogopite (Fig. 4f) and are supposedly of primary origin. Solid inclusions filled by non-chlorite minerals are scarce and are much smaller than those with chlorite. They are associated with core parts of chromite I, whereas chromite II does not contain inclusions.

The non-chlorite inclusions occurring within the Ślęża chromites are mono- and polyphase (Fig. 4). They comprise the following minerals:

a) Clinopyroxene occurs as rounded or irregular-shaped grains. It locally forms intergrowths with pargasite or polyphase inclusions with pargasite and chalcopyrite. Clinopyroxene has diopside composition with high Mg# (93.2–96.1 wt%). It contains 1.47–2.84 wt% Al_2O_3 (Fig. 8, Table 3) and mostly has a low TiO_2 content (< 0.1 wt%) with the exception of one titanium-rich inclusion (0.49–0.57 wt% TiO_2). The Cr_2O_3 contents measured in clinopyroxene (1.18–1.95 wt

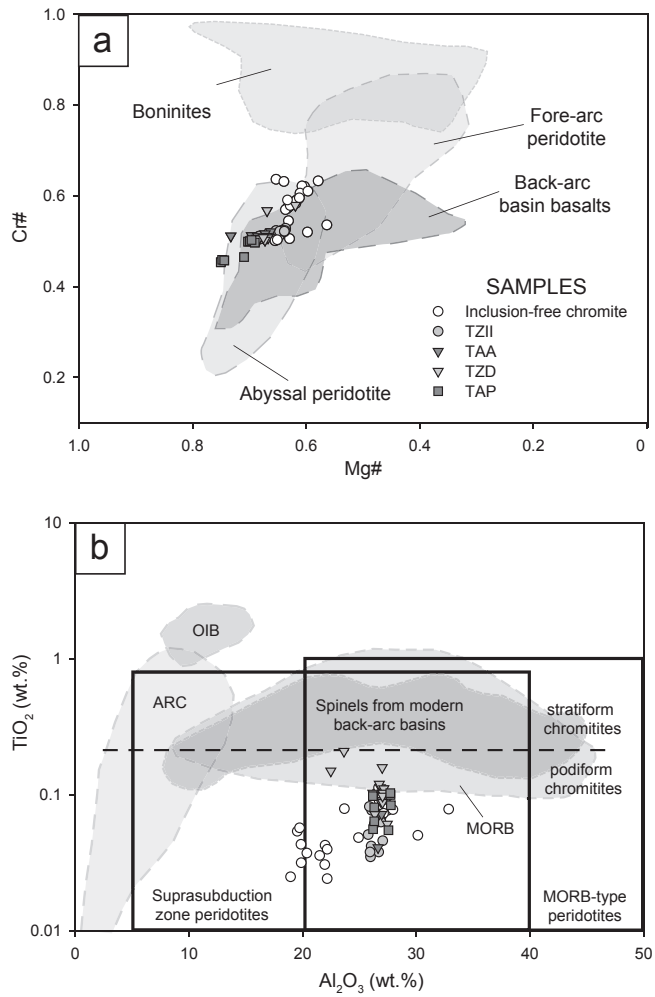

Fig. 6. a - Relationships between Cr# and Mg# in chromites from chromitites of the Czernica Hill area. The fields of abyssal peridotites, fore-arc peridotites, back-arc basin basalts and boninites after the compilation of Kaczmarek et al. (2015 and references therein). b – Chromite TiO_2 versus Al_2O_3 (wt%) diagram. Fields for Cr-spinels from supra-subduction zone peridotites, mid-ocean ridge type peridotites, mid-ocean ridge basalts (MORB), ocean island basalts (OIB) and island-arc tholeites (ARC) are after Kamenetsky et al. (2001).

%) may be partly affected by a composition of the host chromite (Borisova et al., 2018);

b) Pargasite forms individual grains or occurs together with diopside. It has high Mg# (0.93–0.95, Table 4). Two kinds of pargasite can be distinguished by composition: pargasite I has higher TiO_2 (3.26–3.40 wt%) and K_2O (0.46–0.50) and lower Na_2O (2.44–2.47 wt%) contents than pargasite II (0.37–0.87 wt% TiO_2, < 0.02 wt% K_2O and 3.05–3.21 wt% Na_2O).
c) Phlogopite inclusions are spherical or elongated. In contrast to other solid inclusions, which have sharp boundaries with hosting spinel, phlogopite grains are surrounded by a narrow zone consisting of chromite-chlorite intergrowths. Compositionally, phlogopites are K-rich and Na-poor – they contain 7.28–9.60 wt% K_2O and up to 0.67 wt% Na_2O (Table 5).
d) Chalcopyrite occurs in polyphase inclusions with diopside and high-Na pargasite II. It forms grains up to 8 μm in size occurring in marginal parts of inclusions or as very fine (up to 2 μm) grains within diopside;
e) Galena forms individual inclusions up to 20 μm in size. The grains are xenomorphic and occur within both chromite I and II.

4.1.2. Ferrogabbros

Metagabbros sampled from the B-B and D-D zones contain 6.8–14.6% Fe-Ti oxides (Fig. 5). Thus, these rocks can be described as ferrogabbros or as massive ferrogabbros, which are defined as having > 5% or > 10% Fe-Ti oxides, respectively, according to the Natland et al. (1991) nomenclature.

Ferrogabbros display ductile deformation structures represented by mineral folding and local foliation expressed by elongation of mineral grains (Fig. 9a and b). In contrast to oxide-poor metagabbros neighboring the B-B and D-D bodies, opaque minerals in ferrogabbros form xenomorphic and interstitial grains with lobate boundaries. The elongation of Fe-Ti oxides from highly deformed samples is concordant with the deformation trend, although the oxides are not deformed (Figs. 5c and 9b).

Ferrogabbros consist of fine- to medium-grained clinopyroxene, amphiboles and plagioclase. Clinopyroxene has an augite composition, with variable Mg#, Al_2O_3 and Na_2O contents (0.47–0.64, 1.42–6.98 wt % and 0.15–2.25 wt%, respectively, Fig. 10a, Table 3). Clinopyroxene and plagioclase are commonly replaced by amphiboles ranging in composition from Mg-hornblende to Fe-actinolite (Fig. 10b, Table 4) and having variable Mg# (0.33–0.63) and TiO_2 content (0.17–1.28 wt %). Typically, Fe-actinolite is poorer in Na_2O than Mg-hornblende (0.49–0.96 vs. 1.43–2.07 wt%). Plagioclase grains are mostly saussuritized, some grains display polysynthetic twinning. The anorthite constituent is variable (50–77% An, Fig. 10c, Table 6). Subautomorphic apatite grains (up to 100 μm in diameter) are associated with plagioclase domains, whereas xenomorphic ones (up to 200 μm long) occur in the amphibole groundmass. Some ferrogabbros are rich in epidote constituting up to 20% vol. of the sample. Epidote commonly overgrowths clinopyroxene, plagioclase and amphiboles. Sulfides are associated both with amphibole and plagioclase. They form elongated or globular grains consisting of pyrite, locally surrounding chalcopyrite.

Fe-Ti oxides in ferrogabbros occur as the following varieties:

1) Single grains or aggregates of ilmenite (Fig. 5c), locally with dismembered margins. Marginal parts of ilmenite grains are partly replaced by titanite, which also forms exsolutions within ilmenite and fills fissures. The fissures are also filled by amphibole and plagioclase. Ilmenite grains contain small zircon, molybdenite and sphalerite inclusions (up to 10 μm in size). In highly deformed samples, ilmenite is intergrown with plagioclase and amphibole;
2) Aggregates consisting of ilmenite and magnetite. Ilmenite forms homogeneous grains containing zircon and rutile inclusions (up to 20 μm in size). They are xenomorphic, lobate and have rounded margins. Magnetite occurs on marginal parts of ilmenite (Figs. 5d and e, 9c). Locally, magnetite forms individual grains with angular and dismembered margins. All magnetite grains contain trellis, worm-like or sandwich ilmenite exsolutions (Fig. 9f). Elongated types occur in two parallel- and sloping-arranged systems. The margins of some magnetite grains are partly replaced by ilmenite. Fissures are filled by amphibole and plagioclase.
3) Elongated ilmenite grains of various sizes (up to 6 mm long) forming two parallel- and sloping-arranged systems (Fig. 9d and e). Irregular-shaped ilmenite grains up to 150 μm in size occur on their margins. This ilmenite network occurs in the amphibole groundmass, spaces between ilmenite are locally filled by titanite and sulfides (pyrite and chalcopyrite). The margins of these networks resemble the outline of former grains.

Ilmenite has a constant chemical composition irrespective of its mode of occurrence. Its V_2O_3 and MnO contents display weak variability (0.76–0.90 wt% V_2O_3 and 1.08–1.50 wt% MnO – Table 2). Magnetite is very poor in MgO (below the detection limit of the applied method) and MnO (≤0.26 wt). It contains up to 1.61 wt% V_2O_3 and variable TiO_2 (0.16–9.82 wt%) and Al_2O_3 (0.13–1.80 wt%) amounts (Fig. 11, Table 2). Higher TiO_2 contents in magnetite were detected in

Table 2
Representative chemical analyses (wt%) and structural formulae of spinel (sum of cations = 3) and ilmenite (sum of cations = 2) from the Ślęża chromitites and ferrogabbros.

Location	Czernica						Ślęża. B-B zone							
Mineral*	1	1	1	1	2	2	3	3	3	3	4	4	4	4
Sample	TAP	TAA	TAA	TZD	TAA	TZD	TV07	TV07	TV08	TV08	TV07	TV07	TV17	TV17
SiO_2	0.10	0.03	0.03	0.04	0.00	0.01	0.01	0.00	0.02	0.01	0.01	0.00	0.01	0.00
TiO_2	0.21	0.04	0.09	0.10	0.35	0.11	4.25	2.74	0.56	0.16	52.66	52.18	51.39	50.91
Al_2O_3	23.64	26.63	26.98	27.74	14.29	11.70	0.48	0.13	0.92	0.41	0.02	0.04	0.18	0.16
Cr_2O_3	46.46	41.95	42.40	41.26	45.40	46.28	0.06	0.05	0.07	0.02	0.00	0.00	0.01	0.00
V_2O_3	0.21	0.17	0.18	0.08	0.02	0.04	1.17	1.15	1.07	1.28	0.84	0.84	0.81	0.88
FeO[a]	13.11	14.88	13.65	13.53	27.84	30.23	87.09	88.54	90.16	91.34	45.76	45.53	46.76	46.98
MnO	0.25	0.18	0.18	0.20	0.35	0.31	0.14	0.08	0.03	0.00	1.41	1.36	1.10	1.08
NiO	0.10	0.07	0.10	0.14	0.24	0.24	0.00	0.00	0.00	0.00	0.00	0.00	0.00	0.00
MgO	14.70	14.93	15.64	15.76	10.00	9.96	0.01	0.00	0.01	0.01	0.03	0.03	0.02	0.02
CaO	0.19	0.02	0.02	0.02	0.00	0.00	0.00	0.00	0.00	0.00	0.00	0.00	0.00	0.00
Total	99.02	99.03	99.36	98.94	98.52	98.93	93.19	92.70	92.81	93.22	100.71	99.98	100.26	100.03
Ti	0.01	0.00	0.00	0.00	0.01	0.00	0.12	0.08	0.02	0.00	0.99	0.99	0.97	0.96
Al	0.85	0.95	0.95	0.98	0.55	0.45	0.02	0.01	0.04	0.02	0.00	0.00	0.01	0.00
Cr	1.12	1.00	1.00	0.97	1.18	1.21	0.00	0.00	0.00	0.00	0.00	0.00	0.00	0.00
V	0.01	0.00	0.00	0.00	0.00	0.00	0.04	0.04	0.03	0.04	0.02	0.02	0.02	0.02
Fe^{3+}[b]	0.02	0.05	0.04	0.05	0.26	0.34	1.69	1.80	1.89	1.93	0.00	0.00	0.04	0.05
Fe^{2+}	0.32	0.32	0.30	0.29	0.50	0.50	1.12	1.08	1.01	1.00	0.96	0.96	0.95	0.94
Mn	0.01	0.01	0.01	0.01	0.01	0.01	0.00	0.00	0.00	0.00	0.03	0.03	0.02	0.02
Ni	0.00	0.00	0.00	0.00	0.01	0.01	0.00	0.00	0.00	0.00	0.00	0.00	0.00	0.00
Mg	0.67	0.67	0.70	0.70	0.49	0.49	0.00	0.00	0.00	0.00	0.00	0.00	0.00	0.00
Mg#	67.7	67.7	69.9	70.7	49.4	49.4	–	–	–	–	–	–	–	–
Cr#	56.9	51.4	51.3	49.9	68.1	72.6	–	–	–	–	–	–	–	–

* 1 – chromite I, 2 – chromite II, 3 – magnetite, 4 – ilmenite.
[a] Total Fe as FeO.
[b] Calculated by charge balance.

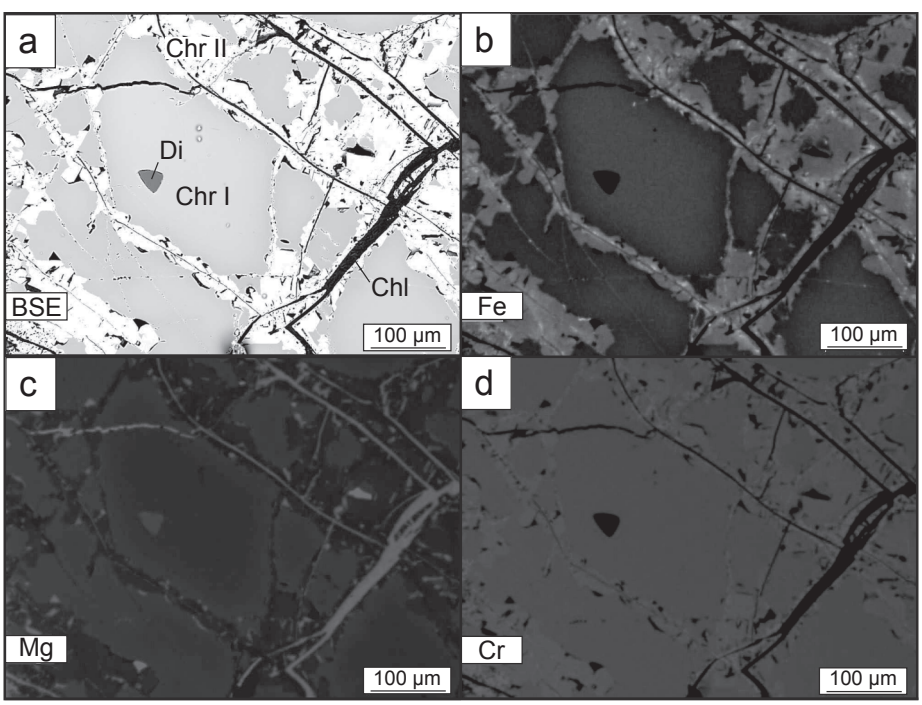

Fig. 7. SEM elemental mapping of chromite grain containing diopside inclusion (TAA). a – BSE image of chromite. b – Fe distribution in chromite. c – Mg distribution in chromite. d – Cr distribution in chromite.

the vicinity of ilmenite exsolutions and may be partly related to the secondary fluorescence coming from ilmenite (Borisova et al., 2018).

4.2. Whole rock composition

Metagabbros from the Ślęża ophiolite differ in terms of silica content (averaged 43.68 wt% SiO_2 in ferrogabbros and 49.36 wt% SiO_2 in isotropic and laminated metagabbros – Table 1). Higher SiO_2 contents correlate positively with Al_2O_3, MgO and CaO and negatively with Fe_2O_3, TiO_2 and MnO. Laminated metagabbros are richer in MgO than isotropic types (averaged 7.81 wt% and 10.41 wt%, respectively). Chemical analyses of metagabbroic pegmatoids define their

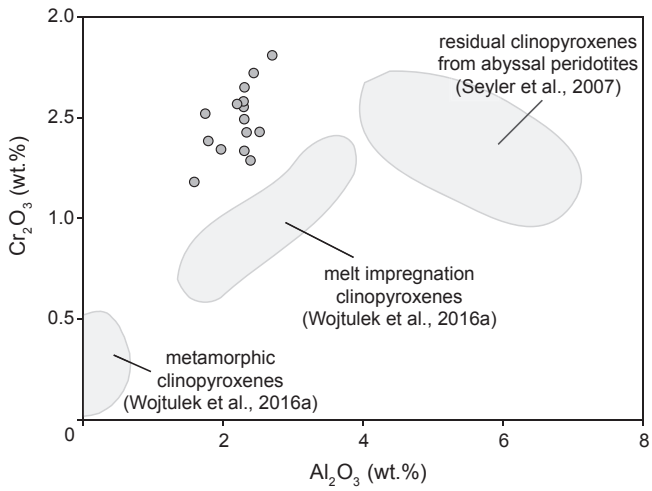

Fig. 8. Cr_2O_3 versus Al_2O_3 (wt%) diagram of clinopyroxene. Fields representing typical compositions of residual (Seyler et al. 2007) and melt impregnation clinopyroxenes (Wojtulek et al., 2016a) are shown for comparison.

composition as intermediate between ferrogabbros and oxide-free metagabbros.

The whole rock compositions reveal higher overall trace element concentrations in ferrogabbros and gabbroic pegmatoids than in oxide-free metagabbros (Fig. 12). Laminated metagabbros have the lowest REE contents. Ferrogabbros, gabbroic pegmatoids and isotropic metagabbros are depleted in REEs, Pb, Zr, Hf and Y and enriched in Rb, Ba and Sr relative to N-MORB (Sun and McDonough, 1989). Their REE patterns are flat in terms of HREE and slightly decrease towards La and Ce. Rare earth elements pattterns of laminated gabbros display a distinct depletion in La, Ce, Pr, Nd and Sm relative to the other REEs. Averaged vanadium contents are notably higher in ferrogabbros (1063 ppm) than in oxide-free metagabbros (174 ppm). Ferrogabbros are extremely poor in all PGEs, whose concentrations are below the detection limit of the applied method. The same refers to Sn, Th and U.

5. Discussion

5.1. Chromitites

5.1.1. Formation of inclusions

The occurrence of inclusions within chromitites from the Ślęża share the following features with rocks from other ophiolitic massifs: (1) the similar mineral composition of inclusions involving hydrous (pargasite, phlogopite) and anhydrous phases (clinopyroxene, Ni-sulfides), (2) the occurrence of inclusions mostly within nodular chromitites, (3) the spherical shape of inclusions, their random arrangement and low abundances within single chromite grains (Fig. 4, cf. Augé, 1987; Melcher et al., 1997). The mode of occurrence of the inclusions is similar to those from the Oman chromitites, which are assumed to have been entrapped contemporaneously with magmatic crystallization of chromite (Lorand and Ceuleneer, 1989).

Nodular texture is an unique feature of ophiolitic chromitites (Matveev and Ballhaus, 2002), suggesting their crystallization from a melt under low-pressure conditions (Cassard et al., 1981; Prichard et al., 2015). The presence of hydrous primary inclusions confirm such conditions, because these phases are typically not stable under higher pressures, e.g. a maximum pressure of pargasite stability in the presence of orthopyroxene amounts 1.2 kbar at 900 °C (Lykins and Jenkins, 1992). Since the assemblage of solid silicate inclusions from the Ślęża chromitites resembles that from the Oman ophiolite, their crystallization conditions were supposedly similar (minerals of an assemblage pargasite-aspidolite-phlogopite from the Oman chromitites crystallized at temperatures ≥700 °C and a maximum pressure of 2 kbar – Borisova et al., 2012). However, the Ślęża chromitites do not comprise aspidolite inclusions, thus a certain estimation of their crystallization conditions is not possible.

5.1.2. Remarks on parental melt and fluid composition

Magmatic models interpreted chromitites as products of crystallization from hydrous, chromite-saturated silicate melts (Irvine, 1975; Lago et al., 1982). However, presence of hydrous inclusions suggests that chromitites were not formed from pure MORB magmas, which are

Table 3
Representative chemical analyses (wt%) and structural formulae (O = 6) of clinopyroxene from the Ślęża chromitites (inclusions) and ferrogabbros.

Location	Chromitites (inclusions)						Ferrogabbros					
Sample	TAA	TAP	TZD	TZD	TZII	TZII	TV07	TV07	TV07	TV08	TV17	TV17
SiO_2	53.27	53.89	53.20	53.57	53.42	53.36	52.86	52.66	52.31	51.99	54.27	51.95
TiO_2	0.04	0.21	0.12	0.22	0.05	0.04	0.15	0.11	0.21	0.20	0.10	0.15
Al_2O_3	2.28	1.57	1.73	2.18	2.32	2.50	3.95	3.75	3.80	2.57	1.79	2.56
Cr_2O_3	1.49	1.18	1.52	1.57	1.43	1.43	0.01	0.00	0.00	0.01	0.01	0.00
FeO*	1.76	1.25	1.34	1.74	1.94	2.03	15.92	15.71	15.92	13.61	16.26	16.25
MnO	0.05	0.08	0.00	0.06	0.04	0.09	0.25	0.23	0.32	0.32	0.20	0.26
NiO	0.00	0.07	0.01	0.05	0.00	0.00	–	–	–	–	–	–
MgO	16.71	17.06	16.91	16.73	17.43	17.39	13.77	13.91	13.64	12.30	13.80	11.41
CaO	24.31	24.34	25.06	23.95	22.78	22.60	11.97	11.78	11.89	18.84	12.75	16.72
Na_2O	0.35	0.47	0.28	0.66	0.41	0.43	0.61	0.54	0.65	0.38	0.22	0.38
K_2O	0.00	0.01	0.00	0.00	0.00	0.00	–	–	–	–	–	–
Total	100.26	100.13	100.17	100.73	99.82	99.87	99.49	98.69	98.74	100.22	99.40	99.68
Si	1.93	1.95	1.94	1.94	1.94	1.94	1.98	1.98	1.97	1.96	2.03	1.98
Ti	0.00	0.01	0.00	0.01	0.00	0.00	0.00	0.00	0.01	0.01	0.00	0.00
Al	0.10	0.07	0.07	0.09	0.10	0.11	0.17	0.17	0.17	0.11	0.08	0.11
Cr	0.04	0.03	0.04	0.04	0.04	0.04	0.00	0.00	0.00	0.00	0.00	0.00
Fe	0.05	0.04	0.04	0.05	0.06	0.06	0.50	0.49	0.50	0.43	0.51	0.52
Mn	0.00	0.00	0.00	0.00	0.00	0.00	0.01	0.01	0.01	0.01	0.01	0.01
Ni	0.00	0.00	0.00	0.00	0.00	0.00	–	–	–	–	–	–
Mg	0.90	0.92	0.92	0.90	0.94	0.94	0.77	0.78	0.77	0.69	0.77	0.65
Ca	0.95	0.95	0.98	0.93	0.89	0.88	0.48	0.48	0.48	0.76	0.51	0.68
Na	0.02	0.03	0.02	0.05	0.03	0.03	0.04	0.04	0.05	0.03	0.02	0.03
K	0.00	0.00	0.00	0.00	0.00	0.00	–	–	–	–	–	–
Mg#	94.4	96.1	95.7	94.5	94.1	93.9	60.6	61.2	60.4	61.7	60.2	55.6

* Total Fe as FeO.

Table 4
Representative chemical analyses (wt%) and structural formulae (O = 23) of amphiboles from the Ślęża chromitites (inclusions) and ferrogabbros.

Location	Chromitites (inclusions)					Ferrogabbros				
Mineral[a]	1	1	1	1	1	2	2	3	3	3
Sample	TZD	TZD	TAP	TAP	TAP	TV07	TV07	TV07	TV17	TV17
SiO_2	43.34	45.83	46.14	46.49	45.82	50.69	50.73	42.71	42.69	43.50
TiO_2	0.57	0.92	0.98	0.87	0.37	0.25	0.31	0.42	1.09	0.98
Al_2O_3	13.10	11.43	11.15	10.78	11.03	5.37	4.90	12.49	11.08	11.22
Cr_2O_3	3.11	2.28	2.28	2.25	2.56	0.00	0.00	0.03	0.02	0.05
FeO[b]	2.28	1.62	1.73	1.66	1.78	16.33	16.43	19.97	22.83	20.92
MnO	0.00	0.00	0.00	0.01	0.04	0.25	0.22	0.22	0.19	0.21
NiO	0.00	0.00	0.00	0.00	0.00	–	–	–	–	–
MgO	18.58	19.21	19.50	19.63	19.46	12.83	12.76	8.19	6.38	7.36
CaO	13.05	12.99	12.90	12.99	13.12	11.86	11.99	11.60	11.93	11.61
Na_2O	3.09	3.21	3.28	3.16	2.92	0.96	0.89	2.07	1.50	1.44
K_2O	0.51	0.01	0.02	0.00	0.02	0.06	0.08	0.31	0.22	0.17
Total	97.64	97.50	98.08	97.84	97.18	98.59	98.30	98.01	97.93	97.46
Si	6.18	6.47	6.48	6.53	6.50	7.38	7.42	6.47	6.56	6.63
Ti	0.06	0.10	0.10	0.09	0.04	0.03	0.03	0.05	0.13	0.11
Al	2.20	1.90	1.85	1.79	1.84	0.92	0.84	2.23	2.00	2.01
Cr	0.35	0.25	0.25	0.25	0.29	0.00	0.00	0.00	0.00	0.01
Fe	0.27	0.19	0.20	0.19	0.21	1.99	2.01	2.53	2.93	2.67
Mn	0.00	0.00	0.00	0.00	0.01	0.03	0.03	0.03	0.02	0.03
Ni	0.00	0.00	0.00	0.00	0.00	–	–	–	–	–
Mg	3.95	4.04	4.08	4.11	4.11	2.79	2.78	1.85	1.46	1.67
Ca	1.99	1.96	1.94	1.96	1.99	1.85	1.88	1.88	1.96	1.89
Na	0.85	0.88	0.89	0.86	0.80	0.27	0.25	0.61	0.45	0.43
K	0.09	0.00	0.00	0.00	0.00	0.01	0.01	0.06	0.04	0.03
Mg#	93.6	95.5	95.3	95.5	95.1	58.3	58.1	42.2	33.3	38.6

[a] 1 – pargasite, 2 – magnesiohornblende, 3 – ferrotschermakite.
[b] Total Fe as FeO.

Table 5
Representative chemical analyses (wt%) and structural formulae (O = 22) of phlogopite from the Ślęża chromitites (inclusions).

Sample	TAP	TAP	T1	T1	T1
SiO_2	39.21	38.85	38.33	38.31	39.10
TiO_2	0.61	0.48	0.46	0.44	0.45
Al_2O_3	17.86	17.81	16.56	16.61	15.83
Cr_2O_3	1.92	2.15	2.17	2.13	1.81
FeO*	0.88	1.02	0.77	0.76	0.91
MnO	0.00	0.00	0.00	0.01	0.02
NiO	0.00	0.00	0.69	0.72	0.68
MgO	24.11	24.55	26.35	26.20	27.20
CaO	0.02	0.01	0.00	0.01	0.07
Na_2O	0.67	0.38	0.07	0.07	0.30
K_2O	7.28	7.37	9.48	9.60	8.13
Total	92.55	92.62	94.88	94.86	94.49
Si	5.56	5.51	5.41	5.42	5.50
Ti	0.06	0.05	0.05	0.05	0.05
Al	2.98	2.98	2.76	2.77	2.62
Cr	0.21	0.24	0.24	0.24	0.20
Fe	0.10	0.12	0.09	0.09	0.11
Mn	0.00	0.00	0.00	0.00	0.00
Ni	0.00	0.00	0.08	0.08	0.08
Mg	5.09	5.20	5.55	5.52	5.70
Ca	0.00	0.00	0.00	0.00	0.01
Na	0.18	0.11	0.02	0.02	0.08
K	1.32	1.33	1.71	1.73	1.46

* Total Fe as FeO.

initially very poor in H_2O and Cr (Delaney et al., 1978; Roeder and Reynolds, 1991). These melts may be enriched in water at subsequent stages of their evolution, when H_2O in aqueous fluids from an external source interacts with water-poor melts to form a final hydrous, hybrid MORB melt (Lorand and Ceuleneer, 1989). Low TiO_2 contents in chromite grains from the Ślęża chromitites (mostly below 0.1 wt% – Fig. 6b) may confirm such origin, because solubility of TiO_2 in mantle fluids is very low (Audétat and Keppler, 2005) and chromite grains crystallizing from hydrothermal solutions are typically poor in Ti (e.g. grains from metasomatic diopsidites from the Oman ophiolite – Arai and Akizawa, 2014).

Water in the mantle may have various origins: (1) remelting of hydrated, shallow lithospheric source due to the rise of a mantle diapir (Benoit et al., 1999), (2) dehydration of hydrous phases from rocks in subduction setting (MacLeod et al., 2013) and (3) hybridization of a MORB with hydrothermal fluids (Borisova et al., 2012). Since the primary chromite grains from the Ślęża chromitites have moderate Cr# (Fig. 6), they were formed from melts in the mid-ocean ridge/back arc basin settings (Kamenetsky et al., 2001). Thus, the third type of water origin suggested by Borisova et al. (2012) seems to be the most probable for chromitites from the Ślęża. These authors suggested three stages of chromitite formation: (1) serpentinization of the oceanic mantle, which was a source of chromium and water, (2) deserpentinization of serpentinized mantle peridotites causing liberation of fluids and (3) assimilation of fluids by MORB melts. However, remnants of the first two stages are not preserved in the Ślęża chromitites, because they comprise neither primary serpentine nor deserpentinization olivine/clinopyroxene inclusions (Fig. 8). These phases were supposedly obliterated during formation and metamorphic alteration of chromitites.

The presence of K- and Na-rich hydrous minerals (phlogopite and pargasite) indicates that the hybridizing fluid was supposedly rich in alkaline ingredients (Lorand and Ceuleneer, 1989). Since these inclusions crystallize at temperatures below 950 °C, this property limits their maximum thermal stability and may imply crystallization of chromite in subsolidus conditions (Augé and Johan, 1988; Borisova et al., 2012).

Other information on the melt/fluid composition is provided by the occurrence of Cu-, Ni- and Pb-sulfides in mono- and polyphase inclusions, which suggest that parental, hybridized melt of the Ślęża chromitites contained sulphur and chalcophile elements (cf. Melcher et al., 1997; Borisova et al., 2012). Although the occurrence of sulfide inclusions is a common feature of ophiolitic chromitites, chalcopyrite is very scarce in these rocks (Lorand and Ceuleneer, 1989; Melcher et al., 1997). Polyphase inclusions containing sulfides offer also a possibility to infer about the mineral crystallization sequence. Since these inclusions are dominated by diopside and pargasite located at the margins

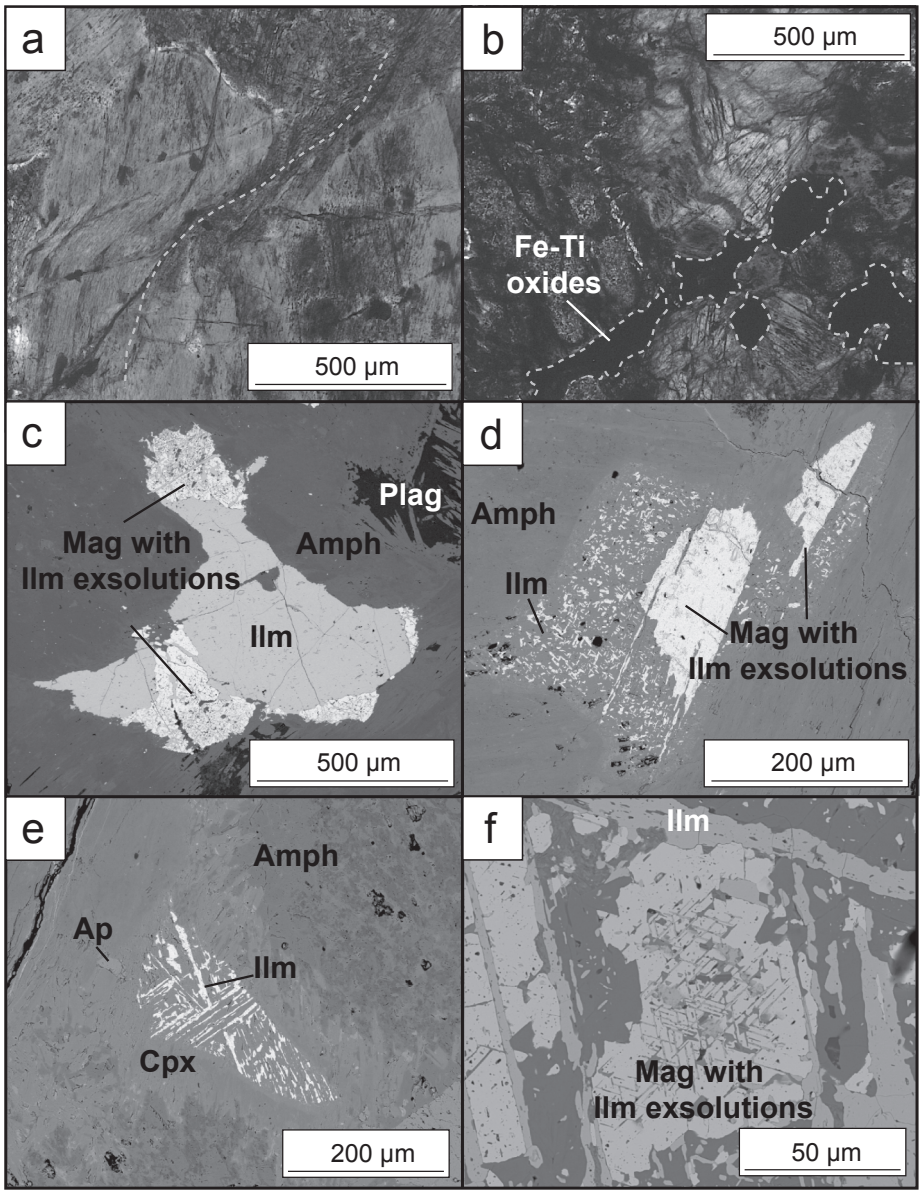

Fig. 9. Photomicrographs of ferrogabbros from the Ślęża ophiolite. a – folded amphibole grains, PPL (TV02). b – deformed rock containing intragrain Fe-Ti oxides, PPL (TV08). c – Ilmenite-magnetite aggregate on amphibole-plagioclase groundmass, BSE image (TV07). d – Fine, elongated ilmenite grains and medium-grained magnetite grains with ilmenite exsolutions on amphibole groundmass, BSE image (TV17). e – Paralel-arranged, elongated ilmenite grains on clinopyroxene, BSE image (TV17). f – Trellis and sandwich ilmenite exsolutions within magnetite, BSE image (TV08).

together with sulfides (Fig. 4d and e), relationships between them suggest that diopside crystallized earlier than pargasite, which is consistent with the higher solidus temperature of diopside (Bowen, 1915).

5.1.3. Metamorphic overprint

Zonation defined by various amounts of Mg and Fe in chromite grains is consistent with a trend of the low-grade metamorphism of chromitites that became depleted in Al and Mg and enriched in Cr and Fe^{3+} (González-Jiménez et al., 2009). Absence of primary, non-chlorite inclusions within chromite II shows that they are very sensitive for metamorphic alteration, which caused their obliteration and replacement by chlorite. Simultaneously, occurrence of primary inclusions within some chromite I grains may indicate that these grains are less altered than those without primary inclusions (Fig. 7).

The preservation of primary solid inclusions suggests that the host chromitites were not significantly altered during post-magmatic deformation and densification processes (Lorand and Ceuleneer, 1989). Presence of pargasite and phlogopite suggest low-grade conditions of chromitite alteration, because during conversion to high-P chromitites hydrous inclusions would breakdown and dissolve in chromite (Yamamoto et al., 2009; Arai, 2013).

5.2. Ferrogabbros

Since ferrogabbros occur within isotropic, oxide-poor gabbros and contact them sharply, they were formed later than their gabbroic host. The flat REE patterns of the ferrogabbros suggests their development from isotropic rocks, which have similar trace element compositions (Fig. 12). This pattern resembles that of N-MORB, thus both ferrogabbros and oxide-free gabbros originated from N-MORB-type melts. Positive Cs, Rb, Ba, Pb and Sr anomalies might imply interaction of gabbros with fluids, since these elements are recognized as fluid mobile elements (Kodolanyi and Pettke, 2011). Laminated gabbros should be excluded as potential precursors for the ferrogabbros, because they display a distinct depletion in some LREEs (La, Ce, Pr, Nd, Sm) relative to other REEs and contain extremely low abundances of Zr and P_2O_5, indicating their more cumulitic character (cf. MacLeod and Yaouancq, 2000).

To obtain an indication of the origin of the magnetites, we plot their composition into the Al-Mn vs. V-Ti discrimination diagram (Fig. 11). Since magnetite has various amounts of Al, Mn, V and Ti, their analyses fall in three fields typical of magmatic porphyry and magmatic Fe-Ti-V deposits, as well as in the field of hydrothermal Kiruna-type deposits.

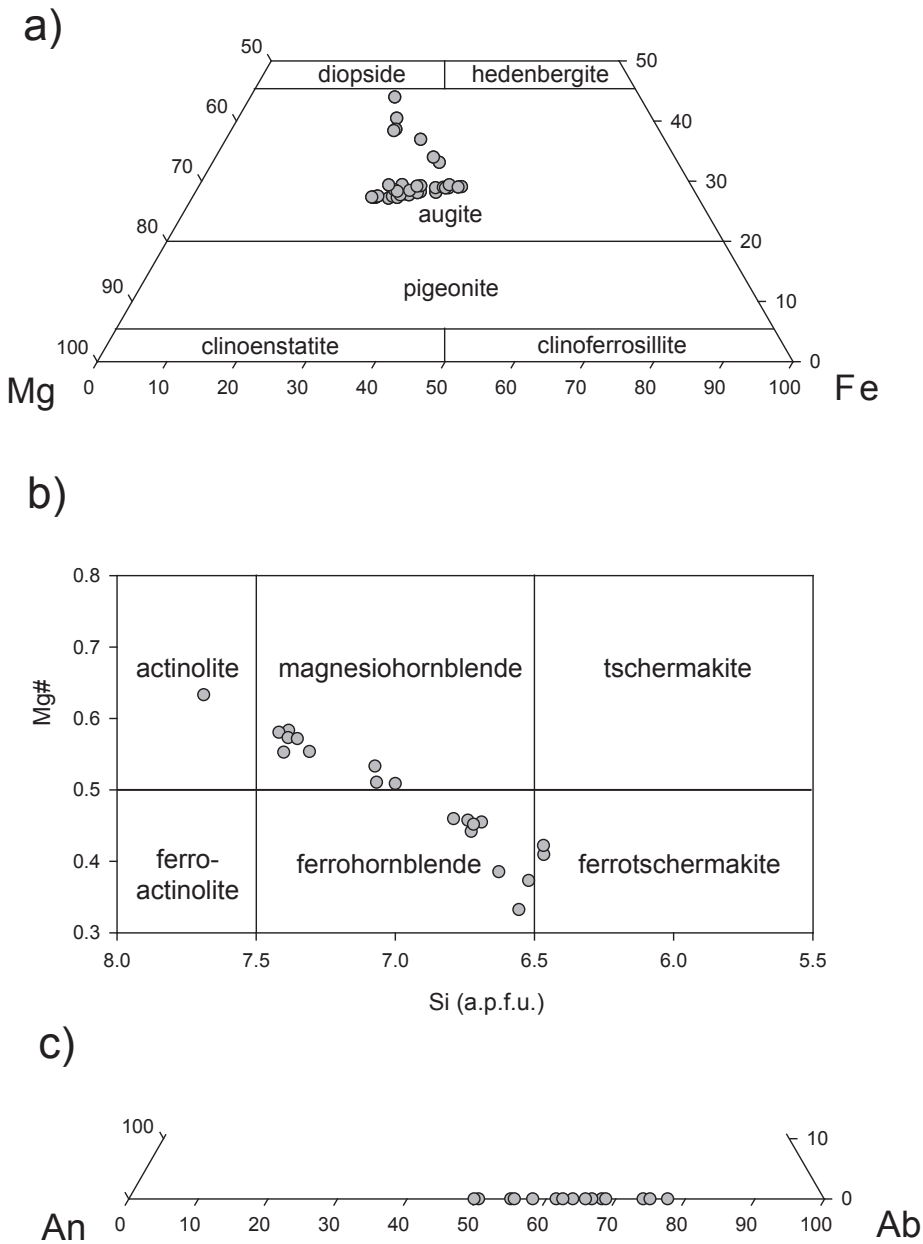

Fig. 10. Composition of clinopyroxene, amphibole and plagioclase from ferrogabbros of the Ślęża ophiolite. a - Classification diagram after Morimoto et al. (1988). b - Classification diagram after Leake et al. (1997). c – Compositional ranges of plagioclase.

Nevertheless, the majority of analyses are as rich in V and Ti as magmatic oxides ones (Dupuis and Beaudoin, 2011; Nadoll et al., 2014). Thus, we interpret magnetite from the ferrogabbros as a magmatic phase, similar to previous suggestions by Niśkiewicz and Siemiątkowski (1993), Majerowicz (2000) and Muszer (2000).

The occurence of magnetite in the marginal parts of the magnetite-ilmenite aggregates and numerous ilmenite exsolutions suggests that magnetite was replaced by ilmenite. Such replacement is related to the removal of Ti from magnetite at subsolidus temperatures due to the oxidation of magnetite–ulvöspinel solid solutions. This process triggers formation of ilmenite and is accompanied by diffusion of Mn towards ilmenite (Buddington and Lindsley, 1964; von Gruenewaldt et al., 1985), which explains high amounts of MnO in ilmenite analyses from the Ślęża ferrogabbros. The lack of magnetite in some samples is supposedly caused by its complete replacement by ilmenite (Fig. 9d). Since ilmenite growth at the expense of magnetite is related mostly to increasing oxygen fugacity, these samples represent the most oxidized ferrogabbros. Subsolidus oxidation of Fe-Ti oxides also intensifies loss of TiO_2 and V_2O_3 (Verhoogen, 1962; Toplis and Corgne, 2002), which explains the lower Ti and V amounts in some magnetite analyses falling in a field of hydrothermal Kiruna in the Al + Mn vs. Ti + V discrimination diagram (Fig. 11).

Xenomorphic textures and the intragranular mode of occurrence of magmatic oxides indicates their formation between silicate grains from melt penetrating the host gabbro. The occurrence of parallel-arranged, elongated ilmenite grains (Fig. 9e and e) suggests that this melt filled also cleavage fissures in the silicate phases. Since both ferrogabbros and the host isotropic gabbros display numerous deformational structures (fissures, foliation, mineral folding), the deformation supposedly affected the conductivity of the gabbros and allowed penetration of melts, similar to deformed oxide-bearing gabbros from the Lizard ophiolite (Hopkinson and Roberts, 1995) and the ODP Leg 176 drilling at the Southwest Indian Ridge (Natland et al., 1991; Agar and Lloyd, 1997; Dick et al., 2000). In these cases, deformation produced an effective

Table 6
Representative chemical analyses (wt%) and structural formulae (O = 5) of plagioclase from the Ślęża ferrogabbros.

Sample	TV07	TV07	TV17	TV17	TV17
SiO_2	57.44	59.74	55.72	62.83	59.79
Al_2O_3	25.87	25.48	25.44	22.87	24.99
FeO*	2.03	0.21	0.35	0.05	0.17
CaO	8.40	8.14	11.91	5.30	7.87
Na_2O	5.77	7.17	6.49	8.74	7.21
K_2O	0.28	0.02	0.00	0.03	0.02
Total	99.77	100.76	99.90	99.82	100.04
Si	2.60	2.65	2.54	2.79	2.67
Al	1.38	1.33	1.36	1.20	1.31
Fe	0.08	0.01	0.01	0.00	0.01
Ca	0.41	0.39	0.58	0.25	0.38
Na	0.51	0.62	0.57	0.75	0.62
K	0.02	0.00	0.00	0.00	0.00
X_{An}	0.44	0.39	0.50	0.25	0.38
X_{Or}	0.02	0.00	0.00	0.00	0.00
X_{Ab}	0.54	0.61	0.50	0.75	0.62

* Total Fe as FeO.

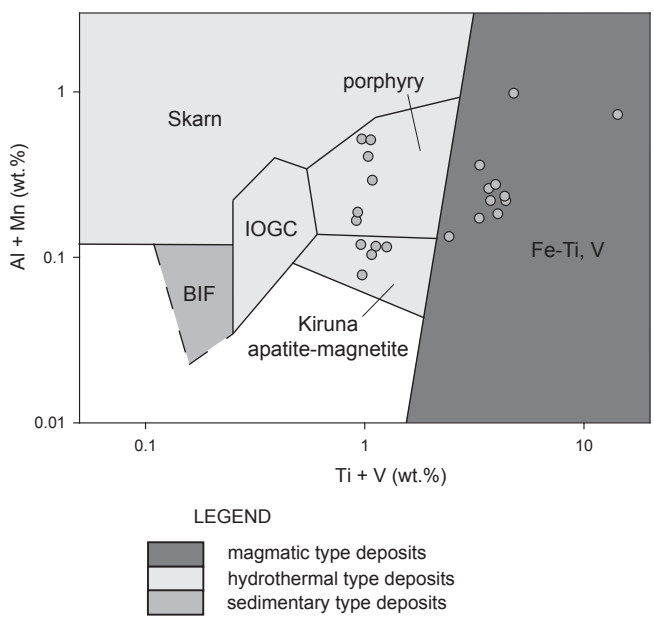

Fig. 11. Al + Mn versus Ti + V (wt%) discriminant diagram for magnetite compositions from ferrogabbros of the Ślęża ophiolite. Fields representing typical compositions of skarn, banded iron formation (BIF), iron-oxide-copper-gold (IOCG), porphyry, apatite-magnetite Kiruna and magmatic Fe-Ti, V deposits (Dupuis and Beaudoin, 2011) are shown for comparison.

porosity used by iron- and titanium-rich, magmatic fractionates developed from melts squeezed during deformation of the gabbros (Natland et al., 1991; Hopkinson and Roberts, 1995). These melts, due to their differentiation, segregated as two silicate liquids with either siliceous or iron-rich compositions which precipitated magmatic Fe-Ti oxides (Natland et al., 1991). Although gabbroic rocks from the Ślęża do not form highly deformed gabbroic mylonites as in the Lizard, crystallization of oxides might follow a similar scenario but at lower deformation intensity.

The occurrence of sulfides as globular or as xenomorphic grains indicates their formation at two stages. Globular shape of grains is widely interpreted as a feature of magmatic sulfides (cf. Miller and Cervantes, 2002; Tomkins et al., 2012). Since these grains in the Ślęża ferrogabbros are associated with silicate minerals, we relate their origin to the crystallization of gabbro. Formation of such sulfides may be related to presence of immiscible Fe-S-O liquids in MORB magmas (Natland et al., 1991). The occurrence of chalcopyrite in sulfide

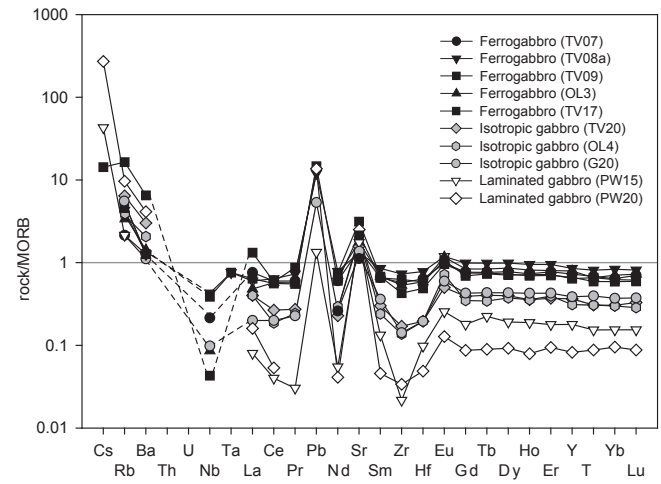

Fig. 12. N-MORB-normalised (Sun and McDonough, 1989) whole-rock trace element patterns of metagabbros from the Ślęża ophiolite.

aggregates suggests also that these liquids were supposedly rich in copper.

The association of xenomorphic sulfide grains with magnetite and ilmenite suggests that crystallization of these sulfides was related to formation of Fe-Ti oxides. Xenomorphic sulfides might crystallized either from the same late melt fractionates as Fe-Ti oxides (cf. Natland et al., 1991) or as phases precipitated from fluids during post-magmatic alteration of ferrogabbros. Crystallization of sulfides from late melts fractionates might be possible after precipitation of Fe-Ti oxides, what caused depletion of these melts in FeO and oxygen and enrichment in sulphur (Mathez, 1976; Perfit and Fornari, 1983).

6. Contrasting formation settings of ore deposits?

In the Ślęża, the harzburgitic mantle and chromitites suggest formation of the mantle section typical of harzburgite ophiolite type (HOT) at intermediate to fast spreading rates (Wojtulek et al., 2016b; Nicolas and Boudier, 2003). However, the crustal plutonic section of the Ślęża does not share features typical for oceanic lithosphere developed at fast spreading conditions. It is composed mostly of isotropic gabbros, whereas the plutonic section of the Oman ophiolite, a classical fast-spreading ophiolite, is predominated by layered gabbros (Pallister and Hopson, 1981). The gabbroic section at the Oman also does not contain ferrogabbros, which are found in lherzolite- or lherzolite-harzburgite ophiolite types (LOT/LHOT), for example the Variscan Lizard and Limousin ophiolites (Hopkinson and Roberts, 1995; Berger et al., 2006; Berger et al., 2010). Thus, the gabbroic member of the Ślęża displays features typical rather of a slow spreading regime, contrasting with the spreading conditions suggested for its mantle section. This difference may suggest that the ultramafic and mafic parts of the Ślęża do not form a continuous ophiolitic sequence.

7. Conclusions

Ultramafic and mafic members of the Variscan Ślęża ophiolite comprise Cr- and Fe-Ti mineralizations. Nodular kind of chromitite ore suggests its formation from a melt under low pressure conditions. Moderate Cr# and presence of hydrous inclusions (pargasite, phlogopite) within chromite grains indicates that the parental melt of chromitites was hydrous and of a MORB affinity. It was enriched in H_2O supposedly due to its interaction with fluids, which caused also a very low TiO_2 content of chromite. Occurrence of hydrous inclusions confirms that presence of fluids is an important factor controlling formation of large chromitite bodies in ophiolites, what is observed in ophiolites of various ages.

The second Fe-Ti mineralization is related to occurrence of ferrogabbros in the Ślęża. High amounts of Al and V in magnetite suggest its magmatic origin. Magnetite grains crystallized supposedly from highly evolved melts of a N-MORB affinity that percolated the deformed, primary gabbroic rocks. Ilmenite forming grains at margins of magnetite aggregates or sandwich/trellis exsolutions within magnetite crystallized supposedly at expense of magnetite due to its subsolidus oxidation. Coexistence of both ferrogabbros and chromitites is an uncommon feature of ophiolites. It may suggest that mafic and ultramafic members of the Ślęża Ophiolite have developed independently.

Acknowledgements

This paper was prepared as a part of an internal project at the University of Wrocław (Ore minerals in ophiolitic rocks from the Central Sudetes, 0420/2290/17) and DAAD (German Academic Exchange Service) fellowship at the TU Bergakademie Freiberg. We thank A.Y. Borisova (University of Toulouse) and an anonymous reviewer for their reviews, which significantly improved this paper. Thanks go to P. Matz (University of Wrocław), S. Gilbricht (TU Bergakademie Freiberg), Dr A. Gąsiński and L. Jeżak (University of Warsaw) for their technical and analytical assistance and to Kamil Bulcewicz and Adam Wojtyna (University of Wrocław) for their assistance during works in the field. Language correction was prepared by Prof. Raymond MacDonald (University of Warsaw).

References

Abdel Wahed, M., Mierzejewski, M., 1998. A new discovery of ilmenite mineralization within the Ślęża Mt. metagabbro, Lower Silesia (SW Poland). Przegląd Geologiczny 46, 684–688 (in Polish, English summary).
Abdel Wahed, M., 1999. The Ślęża Ophiolite (SW Poland): Petrological and Structural Evolution. Ph.D. Thesis. Institute of Geological Sciences, Wrocław University, Poland.
Agar, S.M., Lloyd, G.E., 1997. Deformation of Fe-Ti oxides in gabbroic shear zones from the MARK area. In: Karson, J.A., Cannat, M., Miller, D.J., Elthon, D. (Eds.), Proceedings of the Ocean Drilling Program, Scientific Results, pp. 123–141.
Ahmed, A.H., Arai, S., 2002. Unexpectedly high-PGE chromitite from the deeper mantle section of the northern Oman ophiolite and its tectonic implications. Contrib. Mineral. Petrol. 143, 263–278.
Arai, S., 2013. Conversion of low-pressure chromitites to ultrahigh-pressure chromitites by deep recycling: a good inference. Earth Planet. Sci. Lett. 379, 81–87.
Arai, S., Akizawa, N., 2014. Precipitation and dissolution of chromite by hydrothermal solutions in the Oman ophiolite: new behavior of Cr and chromite. Am. Mineral. 99 (1), 28–34.
Audétat, A., Keppler, H., 2005. Solubility of rutile in subduction zone fluids, as determined by experiments in the hydrothermal diamond anvil cell. Earth Planet. Sci. Lett. 232, 393–402.
Augé, T., 1987. Chromite deposits in the northern Oman ophiolite: mineralogical constraints. Miner. Deposita 22, 1–10.
Augé, T., Johan, Z., 1988. Comparative study of chromite deposits from Troodos, Vourinos, North Oman and New Caledonia ophiolites. In: Boissonnas, J., Omenetto, P. (Eds.), Mineral Deposits within the European Community. Springer, Berlin, pp. 267–288.
Ballhaus, C., Berry, R.F., Green, D.H., 1990. Oxygen fugacity controls in the Earth's upper mantle. Nature 348, 437–440.
Benoit, M., Ceuleneer, G., Polvé, M., 1999. The remelting of hydrothermally altered peridotite at mid-ocean ridges by intruding mantle diapirs. Nature 402, 514–518.
Berger, J., Féménias, O., Mercier, J.-C.C., Demaiffe, D., 2006. A Variscan slow-spreading ridge (MOR-LHOT) in Limousin (French Massif Central): magmatic evolution and tectonic setting inferred from mineral chemistry. Mineral. Mag. 70, 175–185.
Berger, J., Féménias, O., Ohnenstetter, D., Plissart, G., Mercier, J.-C.C., 2010. Origin and tectonic significance of corundum–kyanite–sapphirine amphibolites from the Variscan French Massif Central. J. Metamorph. Geol. 28, 341–360.
Birecki, T., 1962. Occurrence of chromitites at Tąpadła. Przegl. Geol. 10, 144–150 (in Polish with English summary).
Borisova, A.Y., Ceuleneer, G., Kamenetsky, V.S., Arai, S., Béjina, F., Abily, B., Bindeman, I.N., Polvé, M., de Parseval, P., Aigouy, T., Pokrovski, G.S., 2012. A New view on the petrogenesis of the oman ophiolite chromitites from microanalyses of chromite-hosted inclusions. J. Petrol. 53, 2411–2440.
Borisova, A.Y., Zagrtdenov, N.R., Toplis, M.J., Donovan, J., Llovet, X., Asimov, P.D., de Parseval, P., Gouy, S., 2018. Secondary fluorescence effects in microbeam analysis and their impacts on geospeedometry and geothermometry. Chem. Geol. 490, 22–29.
Bowen, N.L., 1915. Crystallization – differentiation in silicate liquids. Am. J. Sci. 39, 175–191.
Buddington, A.F., Lindsley, D.H., 1964. Iron–titanium oxide minerals and synthetic equivalents. J. Petrol. 5, 310–357.
Cassard, D., Nicolas, A., Rabinowicz, M., Moutte, J., Leblanc, M., Prinzhoffer, A., 1981. Structural classification of chromite pods in southern New Caledonia. Econ. Geol. 76, 805–831.
Cholewicka – Meysner D., Farbisz J., Jodłowski S., 1989. Ofiolit Ślęży w świetle badań geofizycznych. In: Ofiolit Ślęży i jego mineralizacja rudna. Wrocław-Sobótka, September 1989, pp. 38–48 (in Polish).
Coleman, R.G., 1977. Ophiolites. Springer, Berlin.
Delaney, J.R., Muenow, D.W., Graham, D.G., 1978. Abundance and distribution of water, carbon and sulfur in the glassy rims of submarine pillow basalts. Geochim. Cosmochim. Acta 42, 581–594.
Delura, K., 2012. Chromitites from the Sudetic ophiolite: origin and alteration. Archivum Mineralogiae Monogr. 4, 1–91.
Dick, H.J.B., Bullen, T., 1984. Chromian spinel as a petrogenetic indicator in abyssaland alpine-type peridotites and spatially associated lavas. Contrib. Mineral. Petrol. 86, 54–76.
Dick, H.J.B., Natland, J.H., Alt, J.C., Bach, W., Bideau, D., Gee, J.S., Haggas, S., Hertogen, J.G.H., Hirth, G., Holm, P.M., Ildefonse, B., Iturrino, G.J., John, B.E., Kelley, D.S., Kikawa, E., Kingdon, A., LeRoux, P.J., Maeda, J., Meyer, P.S., Miller, D.J., Naslund, H.R., Niu, Y.-L., Robinson, P.T., Snow, J., Stephen, R.A., Trimby, P.W., Worm, H.-U., Yoshinobu, A., 2000. A long in situ section of the lower ocean crust: results of ODP Leg 176 drilling at the Southwest Indian Ridge. Earth Planet. Sci. Lett. 179, 31–51.
Dilek, Y., Furnes, H., 2011. Ophiolite genesis and global tectonics: geochemical and tectonic fi ngerprinting of ancient oceanic lithosphere. GSA Bull. 123 (3–4), 387–411.
Dubińska, E., Gunia, P., 1997. The Sudetic ophiolite: current view on its geodynamic model. Geol. Quart. 41 (1), 1–20.
Dubińska, E., Bylina, P., Kozłowski, A., Dörr, W., Nejbert, K., 2004. U – Pb dating of serpentinization: hydrothermal zircon from a metasomatic rodingite shell (Sudetic ophiolite, SW Poland). Chem. Geol. 203, 183–203.
Dupuis, C., Beaudoin, G., 2011. Discriminant diagrams for iron oxide trace element fingerprinting of mineral deposit types. Miner. Deposita 46, 319–335.
Fandrich, R., Gu, Y., Burrows, D., Moeller, K., 2007. Modern SEM-based mineral liberation analysis. Int. J. Miner. Process. 84, 310–320.
Finckh L., 1928, Erläutungen zur geologischen Karte von Preussen 1:25000, Lief. 210, Blatt Zobten, Berlin.
Floyd, P.A., Kryza, R., Crowley, Q.G., Winchester, J.A., Abdel Wahed, M., 2002. Ślęża ophiolite: geochemical features and relationship to Lower Palaeozoic rift magmatism in the Bohemian Massif. Geol. Soc. London Spec. Publ. 201, 197–215.
González-Jiménez, J.M., Kerestedjian, T., Proenza, J.A., Gervilla, F., 2009. Metamorphism on chromite ores from the Dobromirtsi Ultramafic Massif, Rhodope Mountains (SE Bulgaria). Geol. Acta 7, 413–429.
González-Jiménez, J.M., Griffin, W.L., Proenza, J.A., Gervilla, F., O'Reilly, S., Akbulut, M., Pearson, N.J., Arai, S., 2014. Chromitites in ophiolites: how, where, when, why? Part II. The crystallization of chromitites. Lithos 158, 140–158.
Hopkinson, L., Roberts, S., 1995. Ridge axis deformation and coeval melt migration within layer 3 gabbros evidence from the Lizard Complex, UK. Contrib. Mineral. Petrol. 121, 126–138.
Irvine, T.N., 1975. Crystallization sequences in the Muskox intrusion and other layered intrusions – II. Origin of chromitite layers and similar deposits of other magmatic ores. Geochim. Cosmochim. Acta 39, 991–1020.
Jamrozik, L., Niśkiewicz, J., Cholewicka-Meysner, D., Farbisz, J., Jodłowski, S., 1988. Discovery of Fe – Ti mineralized zone in gabbros of the Ślęża massif (Fore-Sudetic Block). Geol. Sudetica 23, 121–127 (in Polish, English summary).
Kaczmarek, M.A., Jonda, L., Davies, H.L., 2015. Evidence of melting, melt percolation and deformation in a suprasubduction zone (Marum Ophiolite Complex, Papua New Guinea). Contrib. Mineral. Petrol. 17. https://doi.org/10.1007/s00410-015-1174-z.
Kamenetsky, V.S., Crawford, A.J., Meffre, S., 2001. Factors controlling chemistry of magmatic spinel: an empirical study of associated olivine, Cr-spinel and melt inclusions from primitive rocks. J. Petrol. 42, 655–671.
Kodolanyi, J., Pettke, T., 2011. Loss of trace elements from serpentinites during fluid-assisted transformation of chrysotile to antigorite – an example from Guatemala. Chem. Geol. 284, 351–362.
Kryza, R., Pin, C., 2002. Mafic rocks in a deep-crustal segment of the Variscides (the Góry Sowie, SW Poland): evidence for crustal contamination in an extensional setting. Int. J. Earth Sci. 91 (6), 1017–1029.
Kryza, R., Pin, C., 2010. The Central-Sudetic ophiolites (SW Poland): petrogenetic issues, geochronology and palaeotectonic implications. Gondwana Res. 17, 292–305.
Lago, B.L., Rabinowicz, M., Nicolas, A., 1982. Podiform chromite ore bodies: a genetic model. J. Petrol. 23, 103–125.
Leake, B.E., Woolley, A.R., Arps, C.E.S., et al., 1997. Nomenclature of amphiboles: report of the Subcommittee on Amphiboles of the International Mineralogical Association Commission on new minerals and mineral names. Mineral. Mag. 61, 295–321.
Leblanc, M., Nicolas, A., 1992. Ophiolitic chromitites. Int. Geol. Rev. 34, 653–686.
Lorand, J.P., Ceuleneer, G., 1989. Silicate and base-metal sulfide inclusions in chromites from the Maqsad area (Oman ophiolite, Gulf of Oman): a model for entrapment. Lithos 22, 173–190.
Lykins, R.W., Jenkins, D.M., 1992. Experimental determination of pargasite stability relations in the presence of orthopyroxene. Contrib. Mineral. Petrol. 112 (2–3), 405–413.
MacLeod, C.J., Yaouancq, G., 2000. A fossil melt lens in the Oman ophiolite: Implications for magma chamber processes at fast spreading ridges. Earth Planet. Sci. Lett. 176, 357–373.
MacLeod, C.J., Lissenberg, C.J., Bibby, L.E., 2013. "Moist MORB" axial magmatism in the Oman ophiolite: The evidence against a mid-ocean ridge origin. Geology 41, 459–462.
Majerowicz, A., 1979. The Ślęża Mt group and ophiolite problems. In: Gunia, T. (Ed.), Field Conference, Septemper 1979, Nowa Ruda, pp. 9–34.

Majerowicz, A., 2000. Some remarks on the ilmenite concentration in the Ślęża ophiolite in the light of petrological studies. Arch. Mineral. 53 (1–2), 61–83.
Majerowicz, A., 2006. Krótki przewodnik terenowy po skałach ofiolitowego zespołu Ślęży oraz ich petrologicznej i geologicznej historii. Acta Universitatis Wratislaviensis 2830, Wrocław 2006 (in Polish).
Mathez, E., 1976. Sulfur solubility and magmatic sulfides in submarine basalt glass. J. Geophys. Res. 81, 4269–4276.
Matveev, S., Ballhaus, C., 2002. Role of water in the origin of podiform chromitite deposits. Earth Planet. Sci. Lett. 203, 235–243.
Mazur, S., Turniak, K., Szczepański, J., McNaughton, N.J., 2015. Vestiges of Saxothuringian crust in the Central Sudetes, Bohemian Massif: zircon evidence of a recycled subducted slab provenance. Gondwana Res. 27, 825–839.
Melcher, F., Grum, W., Simon, G., Thalhammer, T.V., Stumpfl, E.F., 1997. Petrogenesis of the Ophiolitic Giant Chromite Deposits of Kempirsai, Kazakhstan: a Study of Solid and Fluid Inclusions in Chromite. J. Petrol. 38, 1419–1458.
Miller, D.J., Cervantes, P., 2002. Sulfide mineral chemistry and petrography and platinum group element composition in gabbroic rocks from the Southwest Indian Ridge. In: Natland, J.H., Dick, H.J.B., Miller, D.J., Von Herzen, R.P. (Eds.), Proceedings of the Ocean Drilling Program, Scientific Results, pp. 1–29.
Morimoto, N., Fabries, J., Ferguson, A.K., Ginzburg, I.V., Ross, M., Seifert, F.A., Zussman, J., Aoki, K., Gottardi, G., 1988. Nomenclature of pyroxenes. Am. Mineral. 73, 1123–1133.
Muszer, A., 2000. Geneza ilmenitu w rejonie Strzegomian (strefa Strzegomiany – Kunów, Dolny Śląsk). PTMin –. Prace Specjalne 16, 191–209 (in Polish).
Nadoll, P., Angerer, T., Mauk, J.K., French, D., Walshe, J., 2014. The chemistry of hydrothermal magnetite: a review. Ore Geol. Rev. 61, 1–32.
Narębski, W., Wajsprych, B., Bakun-Czubarow, N., 1982. On the nature, origin and geotectonic significance of ophiolites and related rock suites in the Polish part of Sudetes. Ofioliti 2–3, 407–428.
Natland, J.H., Meyer, P.S., Dick, H.J.B., Bloomer, S.H., 1991. Magmatic oxides and sulfides in gabbroic rocks from Hole 735B and the later development of the liquid line of descent. In: Von Herzen, R.P., Robinson, P.T. (Eds.), Proceedings of the Ocean Drilling Program, Scientific Results, pp. 75–111.
Nicolas, A., Boudier, F., 2003. Where ophiolites come from and what they tell us. In: Dilek, Y., Newcomb, S. (Eds.), Ophiolite Concept and the Evolution of Geological Thought, Geological Society of America Special Paper 373.
Niśkiewicz, J., Siemiątkowski, J., 1993. Mineralizacja rudna metagabr strefy Strzegomiany – Kunów (Masyw Ślęży, Dolny Śląsk). Prace Geologiczno-Mineralogiczne XXIII 119–144 (in Polish).
Oliver, G.J.H., Corfu, F., Krough, T.E., 1993. U – Pb ages from SW Poland: evidence for a Caledonian suture zone between Baltica and Gondwana. J. Geol. Soc. London 150, 355–369.
Pallister, J.S., Hopson, C.A., 1981. Samail ophiolite plutonic suite: field relations, phase variation, cryptic variation and layering, and a model of a spreading ridge magma chamber. J. Geophys. Res. 86, 2593–2644.
Perfit, M.J., Fornari, D., 1983. Geochemical studies of abyssal lavas recovered by DSRV Alvin from Eastern Galapagos Rift, Inca Transform, and Ecuador Rift, 2. Phase chemistry and crystallization history. J. Geophys. Res. 88, 10530–10550.
Pin, C., Majerowicz, A., Wojciechowska, I., 1988. Upper Paleozoic oceanic crust in the Polish Sudetes: Nd–Sr isotope and trace element evidence. Lithos 21, 195–209.
Pouchou, J.L., Pichoir, J., 1984. A new model for quantitative X-ray microanalysis. Le Rech Aerospat 3, 167–192.
Prichard, H.M., Barnes, S.J., Godel, B., Reddy, S.M., Vukmanovic, Z., Halfpenny, A., Neary, C.R., Fisher, P.C., 2015. The structure of and origin of nodular chromite from the Troodos ophiolite, Cyprus, revealed using high-resolution X-ray computed tomography and electron backscatter diffraction. Lithos 218–219, 87–98.
Roeder, P.L., Reynolds, I., 1991. Crystallization of chromite and chromium solubility in basaltic melts. J. Petrol. 32, 909–934.
Rospabé, M., Ceuleneer, G., Benoit, M., Abily, B., Pinet, P., 2017. Origin of the dunitic mantle-crust transition zone in the Oman ophiolite: the interplay between percolating magmas and high temperature hydrous fluids. Geology 45, 471–474.
Siivola, J., Schmid, R., 2007. Recommendations by the IUGS Subcommission on the Systematics of Metamorphic Rocks: List of mineral abbreviations. Commission on the Systematics in Petrology. Online version: http://www.bgs.ac.uk/scmr/docs/papers/paper_12.pdf.
Spangenberg, K., 1943. Die Chromerzlagerstätte von Tampadel am Zobten. Zeitschrift für praktische Geologie 51, 25–36.
Sun, S.S., McDonough, W.F., 1989. Chemical and isotopic systematics of oceanic basalts: implications for mantlecomposition and processes. Special Publications 42 In: Saunders, A.D., Norry, M.J. (Eds.), Magmatism in the Ocean Basins. Geological Society, London, pp. 313–345.
Tomkins, A.G., Rebryna, K.C., Weinberg, R.F., Schaefer, B.F., 2012. Magmatic sulfide formation by reduction of oxidized arc basalt. J. Petrol. 53 (8), 1537–1567.
Toplis, M., Corgne, A., 2002. An experimental study of element partitioning between magnetite, clinopyroxene and iron-bearing silicate liquids with particular emphasis on vanadium. Contrib. Mineral. Petrol. 144, 22–37.
Turniak, K., Mazur, S., Domańska-Siuda, J., Szuszkiewicz, A., 2014. SHRIMP U-Pb zircon dating for granitoids from the Strzegom – Sobótka Massif, SW Poland: Constraints on the initial time of Permo-Mesozoic lithosphere thinning beneath Central Europe. Lithos 208–209, 415–429.
Yamamoto, S., Komiya, T., Hirose, K., Maruyama, S., 2009. Coesite and clinopyroxene exsolution lamellae in chromites: in-situ ultrahigh-pressure evidence from podiform chromiites in the Luobusa ophiolite, southern Tibet. Lithos 109, 314–322.
Verhoogen, J., 1962. Oxidation of iron–titanium oxides in igneous rocks. J. Geol. 70, 168–181.
von Gruenewaldt, G., Klemm, D.D., Henckel, J., Dehm, R.M., 1985. Exsolution features in titanomagnetites from massive magnetite layers and their host rocks of the upper zone, eastern Bushveld Complex. Econ. Geol. 80, 1049–1061.
Wojtulek, P.M., Puziewicz, J., Ntaflos, T., 2016a. Melt impregnation phases in the mantle section of the Ślęża ophiolite (SW Poland). Chem. Erde 76, 299–308.
Wojtulek, P.M., Puziewicz, J., Ntaflos, T., Bukała, M., 2016b. Podiform chromitites from the Variscan ophiolite serpentinites of Lower Silesia (SW Poland) – petrologic and tectonic setting implications. Geol. Quart. 60, 56–66.
Wojtulek, P.M., Puziewicz, J., Ntaflos, T., 2017. MORB melt metasomatism and deserpentinization in the peridotitic member of Variscan ophiolite: an example of the Braszowice – Brzeźnica serpentinites (SW Poland). J. Geosci. 62, 147–164.
Znosko, J., 1981. The problem of oceanic crust and of ophiolites in the Sudetes. In: Narębski, W. (Ed.), Ophiolites and Initialites of Northern Border of the Bohemian Massif. Guidebook of Excursions, May-June 1981. vol. II, Potsdam, 3–28.